Eur. Phys. J. C (2010) 70: 155–175
DOI 10.1140/epjc/s10052-010-1471-7

THE EUROPEAN PHYSICAL JOURNAL C

Regular Article - Theoretical Physics

MO analysis of the high statistics Belle results on $\gamma\gamma \to \pi^+\pi^-$, $\pi^0\pi^0$ with chiral constraints

R. García-Martín[1], **B. Moussallam**[2,a]

[1]Departamento de Física Teórica II, Facultad de Ciencias Físicas, Universidad Complutense de Madrid, 28040 Madrid, Spain
[2]Groupe de Physique Théorique, Institut de Physique Nucléaire, Université Paris-Sud 11, 91406 Orsay, France

Received: 5 July 2010 / Published online: 23 October 2010

Abstract We reconsider Muskhelishvili–Omnès (MO) dispersive representations of photon–photon scattering to two pions, motivated by the very high statistics results recently released by the Belle collaboration for charged as well as neutral pion pairs and also by recent progress in the determination of the low-energy $\pi\pi$ scattering amplitude. Applicability of this formalism is extended beyond 1 GeV by taking into account inelasticity due to $K\bar{K}$. A modified MO representation is derived which has the advantage that all polynomial ambiguities are collected into the subtraction constants and have simple relations to pion polarizabilities. It is obtained by treating differently the exactly known QED Born term and the other components of the left-hand cut. These components are approximated by a sum over resonances. All resonances up to spin two and masses up to $\simeq$1.3 GeV are included. The tensor contributions to the left-hand cut are found to be numerically important. We perform fits to the data imposing chiral constraints, in particular, using a model independent sum-rule result on the p^6 chiral coupling c_{34}. Such theoretical constraints are necessary because the experimental errors are dominantly systematic. Results on further p^6 couplings and pion dipole and quadrupole polarizabilities are then derived from the fit. The relevance of the new data for distinguishing between two possible scenarios of isospin breaking in the $f_0(980)$ region is discussed.

1 Introduction

Photon–photon scattering into two pions is a process which probes several aspects of QCD strong dynamics. In particular, as all participating particles are either massless or light, it can probe the low-energy chiral effective theory of QCD. This effective theory has now been worked out up to order p^6 [1, 2]. There are indications that at this order, it can represent the exact dynamics to a very high precision in the two-flavor expansion. This was shown, for instance, for the $\pi\pi$ S-wave scattering lengths (see e.g. the review [3]). Unfortunately, most of the coupling constants of the p^6 chiral Lagrangian are still undetermined. The $\gamma\gamma \to \pi\pi$ amplitude is of particular interest in this respect because of its strong sensitivity to several of these p^6 couplings. Physically, these couplings are associated with electric and magnetic dipole and quadrupole polarizabilities of the pion. These are important observables associated with the structure of the pion. They can be measured, in principle, in Primakov experiments or in photoproduction experiments (apart from low-energy photon–photon scattering). Such experiments have been performed but the present situation is somewhat confused, e.g. the result of MAMI [4] and the preliminary result from COMPASS [5] are not in good agreement, to mention only the most recent experiments.

This paper is motivated by the new experimental measurements by the Belle collaboration of $\gamma\gamma \to \pi\pi$ differential cross sections for charged pions [6, 7] and, very recently, for neutral pions [8, 9]. It becomes thus possible to combine these two complementary sets of measurements in theoretical analysis. There has also been very significant progress, recently, in measuring the $\pi\pi$ scattering amplitude at low energies by the NA48/2 [10–12] the DIRAC [13] and E865 [14] experiments. We will focus here on relating the $\gamma\gamma \to \pi\pi$ experimental results and the low-energy sector of QCD. We will argue that using chiral constraints is useful in analyzing the data and that, in return, chiral information can be extracted from the data. This might appear puzzling at first sight, because Belle's data do not cover the very low-energy region: the $\pi^0\pi^0$ data cover the range $E \gtrsim 0.6$ GeV and the $\pi^+\pi^-$ data the range $E \gtrsim 0.8$ GeV. Extrapolation is possible due to theoretical properties of scattering amplitudes in the standard model, in particular, the property of analyticity of partial-wave amplitudes as a function of energy.

[a] e-mail: moussall@ipno.in2p3.fr

This property, we recall, is a proved consequence of confinement in QCD [15]. Combining with unitarity of the S-matrix enables one to disentangle the effects of the final-state interaction by the Muskhelishvili–Omnès (MO) method [16, 17]. Application to $\gamma\gamma \to \pi\pi$ amplitudes was discussed for the first time in Ref. [18]. Explicit results for $\gamma\gamma \to \pi^+\pi^-$ taking into account current algebra constraints were obtained in [19, 20]. This was reconsidered a few years later [21–23] after the first reliable experimental results in the low-energy region became available. References [22, 23] also discuss how the MO dispersive representation matches with the chiral one-loop representation, which had been computed in Refs. [24, 25] and eventually lead to a parameter free prediction in the low-energy region.

A simplifying feature of low energy is that $\pi\pi$ scattering can be considered elastic. If one is interested in the 1 GeV region or slightly above, it becomes necessary to take inelasticity into account. This is feasible due to a specific feature of $\pi\pi$ scattering: the fact that inelastic scattering to 4π or 6π states (which are not treatable by MO methods) are suppressed in practice and can be neglected up to $E \simeq 1.2$–1.3 GeV. The remaining relevant inelastic channels, $K\bar{K}$ or $\eta\eta$, are two-body channels which are perfectly treatable, in principle, by MO methods. In this paper, we take into account $\pi\pi \to K\bar{K}$ scattering, which is particularly important in the $I = 0$ S-wave near 1 GeV. This amplitude suffers from a long lasting unresolved experimental discrepancy very near the $K\bar{K}$ threshold which limits the determination of the properties of the $f_0(980)$ scalar meson. It is interesting that this discrepancy can be interpreted in terms of two different scenarios for isospin breaking. We will discuss the relevance of Belle's results near 1 GeV in eventually clarifying this issue.

Application of the multichannel MO method to $\gamma\gamma \to \pi\pi$ has been attempted first in Ref. [26] and then discussed in some detail in Ref. [27]. More recently, it was applied to Belle's data on $\pi^+\pi^-$ in Ref. [28]. These authors have considered the extrapolation of the amplitude in the complex plane, so as to define, and then extract, the couplings of the scalar mesons $\sigma(600)$ and $f_0(980)$ to two photons. Determination of these couplings has aroused sustained interest in the literature (e.g. [29–33], a more complete list can be found in [28]). One motivation is to probe the structure of scalar mesons and identify the glueballs. There is some scatter in the results obtained. In the present paper, we concentrate on extrapolating on the real axis, toward the low-energy region. This brings constraints on the amplitude which should prove useful also for extrapolating away from the real axis. This will be discussed elsewhere.

The plan of the paper is as follows. After introducing notation for the amplitudes and their partial-wave expansions we write the unitarity equations in the one- and two-channel approximations. Next, we formulate the MO-type dispersive representations. Concerning the left-hand cut, we find it advantageous to treat differently the QED Born term and the multipion contributions in the MO representations. The latter are kept in the form of a subtracted left-cut spectral integral. We then implement the (usual) approximation of retaining only resonance contributions. All resonances with mass up to $\approx$1.3 GeV are included and we show that a certain regulation operates between resonances of different spin and different parity depending on the helicity states. Subtractions at $s = 0$ are introduced in the MO dispersive representations in order to suppress higher energy regions in the integrands where our truncated unitarity equations no longer apply. The subtraction constants have simple relations to dipole and quadrupole pion polarizabilities and are to be determined from fits to the data. Chiral constraints may be applied to the fit. This is necessary because the errors in Belle's data are completely dominated by systematics and the usual statistical interpretation of the χ^2 does not apply, strictly speaking. Only one of the relevant p^6 chiral coupling constants is known in a model independent way from a chiral sum rule. We show that this information implies a relation between dipole and quadrupole polarizabilities of the neutral pion which we implement in the fit. Then, we describe our inputs for the $\pi\pi \to \pi\pi$, $K\bar{K}$ T-matrix elements. Our subtracted dispersive integrals emphasize the low-energy part of the integrands. We employ a parametrization which allow for some freedom near the $K\bar{K}$ threshold since the Belle data probe this region in some detail. Finally, we display comparisons between the fitted MO amplitudes and the experimental data and discuss the implication for the pion polarizabilities and the p^6 chiral coupling constants.

2 Kinematics, unitarity relations

We consider the processes $\gamma(q_1,\lambda)\gamma(q_2,\lambda') \to \pi^+(p_1)\pi^-(p_2)$ or $\pi^0(p_1)\pi^0(p_2)$ where $\lambda(\lambda') = \pm 1$ are the photons helicities. We will also consider $\gamma(q_1,\lambda) \times \gamma(q_2,\lambda') \to K(p_1)\bar{K}(p_2)$ with $I = 0$ which plays a role in the S-wave via coupled channel unitarity. We take the Mandelstam invariants as

$$s = (q_1+q_2)^2, \qquad t = (q_1-p_1)^2, \qquad u = (q_1-p_2)^2 \quad (1)$$

which satisfy $s + t + u = 2m_\pi^2$. The physical regions in the Mandelstam plane for $\gamma\gamma \to 2\pi$ and for the crossed-channel amplitude $\gamma\pi \to \gamma\pi$ are shown in Fig. 1. The scattering angle θ in the two photon center-of-mass system is related as follows to s, t, u:

$$\cos\theta = \frac{t-u}{\sqrt{s(s-4m_\pi^2)}}. \quad (2)$$

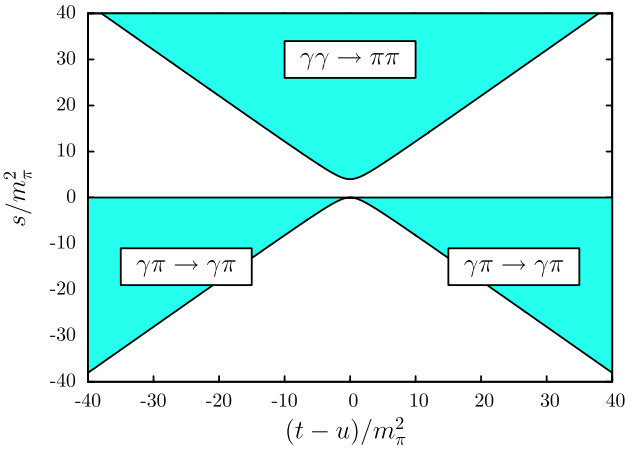

Fig. 1 Mandelstam plane showing the physical regions for $\gamma\gamma \to 2\pi$ and $\gamma\pi \to \gamma\pi$ processes

We write the S-matrix element for $\gamma\gamma \to \pi^+\pi^-$ as

$$\begin{aligned}&\big\langle_{\text{out}}\pi^+(p_1)\pi^-(p_2)|\gamma(q_1,\lambda)\gamma(q_2,\lambda')\big\rangle_{\text{in}}\\&\quad= ie^2(2\pi)^4\delta^4(P_f-P_i)\mathrm{e}^{i(\lambda-\lambda')\phi}H^c_{\lambda\lambda'}(s,t)\end{aligned}\tag{3}$$

factoring out e^2 as well as the explicit dependence on the azimuthal angle ϕ. With this convention, $H^c_{\lambda\lambda'}$ is a function of the Mandelstam variables. Similarly, in the case of $\gamma\gamma \to \pi^0\pi^0$ we denote the scattering amplitude by $H^n_{\lambda\lambda'}$. In the case of $\gamma\gamma \to K\bar{K}$ scattering we denote the charged and neutral amplitudes by $K^c_{\lambda\lambda'}$ and $K^n_{\lambda\lambda'}$ respectively. We assume that isospin is exactly conserved by the strong interaction. It is then useful to consider the amplitudes which correspond to $\pi\pi$ or $K\bar{K}$ final states with definite isospin I. We will label them as $H^I_{\lambda\lambda'}$ and $K^I_{\lambda\lambda'}$. Because of parity conservation, only final states with even values of the angular momentum J are allowed, $J = 0, 2, 4, \ldots$. Invoking also charge conjugation invariance the isospin values must be $I = 0$ or $I = 2$ in the case of $\pi\pi$, while in the case of $K\bar{K}$ both $I = 0$ and $I = 1$ can couple to $\gamma\gamma$. The relations between the amplitudes $\gamma\gamma \to \pi^+\pi^-, \pi^0\pi^0$ and the isospin ones $\gamma\gamma \to (\pi\pi)_{I=0,2}$ read

$$\begin{pmatrix}\sqrt{2}H^c_{\lambda\lambda'}\\ H^n_{\lambda\lambda'}\end{pmatrix}=\begin{pmatrix}-\sqrt{\frac{2}{3}} & -\sqrt{\frac{1}{3}}\\ -\sqrt{\frac{1}{3}} & \sqrt{\frac{2}{3}}\end{pmatrix}\begin{pmatrix}H^0_{\lambda\lambda'}\\ H^2_{\lambda\lambda'}\end{pmatrix}.\tag{4}$$

In the case of kaons, the analogous relations read,

$$\begin{pmatrix}K^c_{\lambda\lambda'}\\ K^n_{\lambda\lambda'}\end{pmatrix}=\begin{pmatrix}-\sqrt{\frac{1}{2}} & -\sqrt{\frac{1}{2}}\\ -\sqrt{\frac{1}{2}} & \sqrt{\frac{1}{2}}\end{pmatrix}\begin{pmatrix}K^0_{\lambda\lambda'}\\ K^1_{\lambda\lambda'}\end{pmatrix}.\tag{5}$$

It is useful to carry out a tensorial decomposition of the photon–photon scattering amplitudes. Writing

$$H_{\lambda\lambda'}(q_i,p_i)=\epsilon_1^\mu(\lambda)\epsilon_2^\nu(\lambda')W_{\mu\nu}(p_i,q_i)\tag{6}$$

where ϵ_i are the polarization vectors of the photons. $W_{\mu\nu}$ can be decomposed as

$$W_{\mu\nu}=A(s,t,u)T_{1\mu\nu}+B(s,t,u)T_{2\mu\nu}\tag{7}$$

where

$$\begin{aligned}T_{1\mu\nu}&=\frac{1}{2}s\,g_{\mu\nu}-q_{1\nu}q_{2\mu},\\T_{2\mu\nu}&=2s\Delta_\mu\Delta_\nu-(t-u)^2g_{\mu\nu}\\&\quad-2(t-u)(q_{1\nu}\Delta_\mu-q_{2\mu}\Delta_\nu)\end{aligned}\tag{8}$$

where $\Delta = (p_1 - p_2)$. In this manner, the Ward identities are satisfied as follows:

$$q_1^\mu W_{\mu\nu}=q_2^\nu W_{\mu\nu}=0.\tag{9}$$

The functions A and B satisfy analyticity properties as a function of s, t, u and they are symmetric under crossing $(t,u) \to (u,t)$ (because of Bose symmetry of the two photon system). One can express the helicity amplitudes in terms of A and B as follows:[1]

$$\begin{aligned}H_{++}&=H_{--}=\frac{1}{2}sA-s\big(s-4m_\pi^2\big)B,\\H_{+-}&=H_{-+}=4\big(tu-m_\pi^4\big)B.\end{aligned}\tag{10}$$

Finally, the differential cross section for $\gamma\gamma \to \pi\pi$ has the following expression:

$$\frac{d\sigma}{d\Omega}=\frac{\alpha^2}{8s}\beta_\pi(s)\big(|H_{++}|^2+|H_{+-}|^2\big)\tag{11}$$

with

$$\beta_\pi(s)=\sqrt{1-\frac{4m_\pi^2}{s}}.\tag{12}$$

2.1 Partial-wave expansions

In order to perform the partial-wave expansion for helicity amplitudes we use the Jacob and Wick [35] formulas,

$$\begin{aligned}&\langle\theta\phi\lambda_c\lambda_d|T|0,0,\lambda_a\lambda_b\rangle\\&\quad=N\sum_J(2J+1)D^{*J}_{\lambda_a-\lambda_b,\lambda_c-\lambda_d}(\theta,\phi)\langle\lambda_c\lambda_d|T_J|\lambda_a\lambda_b\rangle\end{aligned}\tag{13}$$

where N is a normalization factor which can be chosen arbitrarily. Let us list below the partial-wave expansions for all

[1] The polarization vectors are chosen in accordance with the phase convention of Edmonds [34] for spherical tensors.

the scattering amplitudes which are relevant in our work,

$$\begin{aligned}
&\gamma\gamma \to \pi\pi: \quad H^I_{\lambda\lambda'} = \sum (2J+1) h^I_{J,\lambda\lambda'}(s) d^J_{\lambda-\lambda',0}(\theta),\\
&\gamma\gamma \to K\bar{K}: \quad K^I_{\lambda\lambda'} = \frac{1}{\sqrt{2}} \sum (2J+1) k^I_{J,\lambda\lambda'}(s)\\
&\qquad\qquad \times d^J_{\lambda-\lambda',0}(\theta),\\
&\pi\pi \to \pi\pi: \quad F^I = 32\pi \sum (2J+1) f^I_J(s) d^J_{00}(\theta),\\
&\pi\pi \to K\bar{K}: \quad G^I = 16\sqrt{2}\pi \sum (2J+1) g^I_J(s) d^J_{00}(\theta),\\
&K\bar{K} \to K\bar{K}: \quad R^0 = 16\pi \sum (2J+1) r^0_J(s)\, d^J_{00}(\theta).
\end{aligned} \tag{14}$$

The different normalization factors are chosen such as to ensure simple formulas for the unitarity relations satisfied by the partial-wave amplitudes. The general unitarity relation reads, for a given T-matrix element

$$T_{fi} - T^*_{if} = i \sum_n T^*_{nf} T_{ni}. \tag{15}$$

If the energy is sufficiently small, the sum over intermediate states is limited to just one state, $\pi\pi$ (elastic unitarity). We will consider this to be a reasonably good approximation for our purposes except in the $I = 0$, $J = 0$ case (see Sect. 3). At the level of the partial waves, if $J \neq 0$ or $I \neq 0$ we then have

$$\operatorname{Im} h^I_{J,\lambda\lambda'}(s) = \theta\big(s - 4m_\pi^2\big) \beta_\pi(s) f^I_J(s) h^{*I}_{J,\lambda\lambda'}(s). \tag{16}$$

For $I = 0$ $J = 0$ we also include $K\bar{K}$ in the sum (15). The unitarity relation can be written in matrix form

$$\begin{pmatrix} \operatorname{Im} h^0_{0,++}(s) \\ \operatorname{Im} k^0_{0,++}(s) \end{pmatrix} = T\Sigma \begin{pmatrix} h^{*0}_{0,++}(s) \\ k^{*0}_{0,++}(s) \end{pmatrix} \tag{17}$$

with

$$\begin{aligned}
T &= \begin{pmatrix} f^0_0(s) & g^0_0(s) \\ g^0_0(s) & r^0_0(s) \end{pmatrix},\\
\Sigma &= \begin{pmatrix} \theta(s - 4m_\pi^2)\beta_\pi(s) & 0 \\ 0 & \theta(s - 4m_K^2)\beta_K(s) \end{pmatrix}.
\end{aligned} \tag{18}$$

3 (Modified) Omnès–Muskhelishvili representations

The partial-wave photon–photon scattering amplitudes $h^I_{J,\lambda\lambda'}(s)$ are analytic functions of the variable s with two cuts on the real axis: (1) a right-hand cut extending from $4m_\pi^2$ to ∞ and (2) a left-hand cut extending from $-\infty$ to 0. The discontinuity along the right-hand cut is given by the unitarity relations (16), (17). These properties are the basis of the Muskhelishvili–Omnès (MO) method for treating the final-state interaction problem, which has been applied for the first time to the $\gamma\gamma \to \pi\pi$ scattering amplitudes by Gourdin and Martin [18]. The usual method [16] is based on writing a dispersion relation for the function,

$$\tilde{F}(s) \equiv \Omega^{-1}(s)\big[F(s) - F_L(s)\big] \tag{19}$$

where F is the amplitude of interest, F_L the part of this amplitude which has a left-hand cut and Ω is the Omnès function. The function $\tilde{F}(s)$, by construction, has only a right-hand cut. We will use a slightly modified version here, which treats on a different footing the part of the left-hand cut associated with the QED Born term (which is known exactly) and the remaining part, which we will associate with resonance exchanges. Instead of (19), we will consider

$$\tilde{F}_{\rm mod}(s) \equiv \Omega^{-1}(s)\big[F(s) - F^{\rm Born}_L(s)\big] \tag{20}$$

i.e. we subtract only the Born term piece such that the function $\tilde{F}_{\rm mod}(s)$ has both a right-hand cut and a left-hand cut. A simplification arising in this modified approach is that all polynomial terms are absorbed into the subtraction constants of the dispersive representation.

In practice, in order to evaluate the imaginary part of $\tilde{F}(s')$ (or $\tilde{F}_{\rm mod}(s')$) on the right-hand cut, which is needed in the dispersion relation, one sets $\operatorname{Im}[\Omega^{-1}(s')F(s')]$ equal to zero in (19), (20). This is exact in the energy region where scattering is elastic but becomes inaccurate at higher energies. The influence of this inaccuracy can be reduced by writing down over-subtracted dispersion relations, so as to suppress the integrand in the inelastic region. With this in mind, it also makes sense to define the Omnès function over an infinite range, making a plausible guess[2] concerning the behavior of the phase-shift as $s' \to \infty$. Alternatively, one could perform all the dispersive integrations over a finite range $s' \leq s_c$ and approximate the contributions from the range $s' > s_c$ by polynomials with unknown coefficients. This should be practically equivalent to the procedure adopted here. In the end, the sensitivity of the results on the higher energy ranges of the various integrals would have to be included in the errors.

Let us now consider the MO representations in more detail.

- *S*-**wave** $I = 0$

[2] To be more specific, we assume that $I = 2$ phase-shifts tend to zero. For $I = 0$ and $J = 0$ we take: $\lim_{s\to\infty} \delta_{\pi\pi}(s) = 2\pi$, $\lim_{s\to\infty} \delta_{KK}(s) = 0$ and $\lim_{s\to\infty} |T_{\pi\pi\to K\bar{K}}(s)| = 0$ while for $I = 0$ and $J = 2$ we assumed that the phase-shift goes to π.

For the $I=0$ S-wave, it is necessary to generalize the MO representation to two channels in order to properly describe the $f_0(980)$ resonance energy region. The Omnès function must be replaced by a 2×2 Omnès matrix

$$\overline{\overline{\Omega}}(s)=\begin{pmatrix}\Omega_{11}(s) & \Omega_{12}(s)\\ \Omega_{21}(s) & \Omega_{22}(s)\end{pmatrix}. \tag{21}$$

The matrix elements of the Omnès matrix are analytic functions of s with only a right-hand cut as in the one-channel case. The discontinuities along this cut are given, in terms of the 2×2 T-matrix, by equations analogous to (17) that read,

$$\operatorname{Im}\overline{\overline{\Omega}}(s)=T\Sigma\overline{\overline{\Omega}}^{*}(s). \tag{22}$$

Unlike the one-channel case, the MO equations have no known analytic solutions for two or more channels [17], but accurate numerical solutions can be constructed [36, 37]. The MO representation couples $\gamma\gamma\to(\pi\pi)_{I=0}$ S-wave amplitude and the $\gamma\gamma\to(K\bar{K})_{I=0}$ S-wave amplitude. We write, a priori, a representation which involves four subtraction parameters

$$\begin{aligned}&\begin{pmatrix}h^0_{0,++}(s)\\ k^0_{0,++}(s)\end{pmatrix}\\ &=\begin{pmatrix}\bar{h}^{0,\mathrm{Born}}_{0,++}(s)\\ \bar{k}^{0,\mathrm{Born}}_{0,++}(s)\end{pmatrix}+\overline{\overline{\Omega}}(s)\left[\begin{pmatrix}b^{(0)}s+b'^{(0)}s^2\\ b^{(0)}_K s+b'^{(0)}_K s^2\end{pmatrix}\right.\\ &\quad+\frac{s^3}{\pi}\int_{-\infty}^{-s_0}\frac{ds'}{(s')^3(s'-s)}\overline{\overline{\Omega}}^{-1}(s')\operatorname{Im}\begin{pmatrix}\bar{h}^{0,\mathrm{Res}}_{0,++}(s')\\ \bar{k}^{0,\mathrm{Res}}_{0,++}(s')\end{pmatrix}\\ &\quad\left.-\frac{s^3}{\pi}\int_{4m_\pi^2}^{\infty}\frac{ds'}{(s')^3(s'-s)}\operatorname{Im}\overline{\overline{\Omega}}^{-1}(s')\begin{pmatrix}\bar{h}^{0,\mathrm{Born}}_{0,++}(s')\\ \bar{k}^{0,\mathrm{Born}}_{0,++}(s')\end{pmatrix}\right].\end{aligned} \tag{23}$$

As usual, subtraction constants have been set equal to zero in order to comply with the soft-photon theorem [38–40] near $s=0$ e.g.

$$h^0_{0,++}(s)-\bar{h}^{0,\mathrm{Born}}_{0,++}(s)=O(s). \tag{24}$$

The left-cut functions $\bar{h}^{0,\mathrm{Born}}_{0,++}(s')$, $\bar{k}^{0,\mathrm{Born}}_{0,++}(s')$, $\bar{h}^{0,\mathrm{Res}}_{0,++}(s')$ and $\bar{k}^{0,\mathrm{Res}}_{0,++}(s')$ which enter into this representation will be given explicitly in Sect. 4.

Due to the property of real analyticity the discontinuity of the amplitude $h^0_{0,++}(s)$ across the right-hand cut is expressed in terms of a phase ϕ_{00}

$$h^0_{0,++}(s+i\epsilon)=e^{2i\phi_{00}(s)}h^0_{0,++}(s-i\epsilon),\quad \left(s\geq 4m_\pi^2\right) \tag{25}$$

This phase is equal (modulo π) to the $\pi\pi$ phase-shift below the $K\bar{K}$ threshold by Watson's theorem. The representation given above provides a modeling of ϕ_{00} above the $K\bar{K}$ threshold (depending on the polynomial parameters) which is plausible below the effective onset of 4π inelasticity. The amplitude $h^0_{0,++}(s)$ satisfies a one-channel Omnès representation in terms of the Omnès function associated with ϕ_{00} and two polynomial parameters. We have verified this property as a check of our numerical calculations.

• *S*-**wave** $I=2$

In this case, $K\bar{K}$ inelasticity is not allowed. We will then disregard inelasticity in the energy region of interest. We write an MO representation with two subtraction constants

$$\begin{aligned}h^2_{0,++}(s)=\bar{h}^{2,\mathrm{Born}}_{0,++}(s)+\Omega^2_0(s)\Bigg[&b^{(2)}s+b'^{(2)}s^2\\ &+\frac{s^3}{\pi}\int_{-\infty}^{-s_0}\frac{\operatorname{Im}\bar{h}^{2,\mathrm{Res}}_{0,++}(s')}{\Omega^2_0(s')(s')^3(s'-s)}ds'\\ &+\frac{s^3}{\pi}\int_{4m_\pi^2}^{\infty}\frac{\sin\delta^2_0(s')\,\bar{h}^{2,\mathrm{Born}}_{0,++}(s')}{|\Omega^2_0(s')|(s')^3(s'-s)}ds'\Bigg].\end{aligned} \tag{26}$$

Here $\delta^2_0(s)$ is the $I=2$ $\pi\pi$ phase-shift and the Omnès function is given in terms of $\delta^2_0(s)$ by

$$\Omega^2_0(s)=\exp\left(\frac{s}{\pi}\int_{4m_\pi^2}^{\infty}\frac{\delta^2_0(s')}{s'(s'-s)}ds'\right). \tag{27}$$

• *D*-**waves** $I=0$ **and** $I=2$

In the $I=0$ case, the partial-wave analysis performed by Hyams et al. [41] found the inelasticity around the $f_2(1270)$ peak to be of the order of 30%. The PDG [42] now quotes a smaller value, approximately 15%, of which only 5% is due to $K\bar{K}$, the remaining part being due to 4π. We will therefore not attempt a coupled channel description in this case and essentially ignore the inelasticity. In the $I=2$ case, the final-state interaction is very small and will also ignore the inelasticity. The Omnès method differs from that discussed above only by the fact that we must account properly for centrifugal barrier factors. At small energies, indeed, it is not difficult to see that the amplitudes with $J=2$ should behave as follows:

$$\begin{aligned}&h^I_{2,++}(s)-\bar{h}^{I,\mathrm{Born}}_{2,++}(s)\sim s^2\left(s-4m_\pi^2\right),\\ &h^I_{2,+-}(s)-\bar{h}^{I,\mathrm{Born}}_{2,+-}(s)\sim s\left(s-4m_\pi^2\right).\end{aligned} \tag{28}$$

This is implemented by multiplying the Omnès function by $(s-4m_\pi^2)$ and by setting the appropriate subtraction constants to zero in the dispersive representation. One then ob-

tains,

$$h^I_{2,++}(s) = \bar{h}^{I,\mathrm{Born}}_{2,++}(s) + \Omega^I_2(s)s^2\big(s-4m_\pi^2\big) \times\left[c^{(I)} + \frac{s}{\pi}\int_{-\infty}^{-s_0}\frac{\mathrm{Im}\,\bar{h}^{I,\mathrm{Res}}_{2,++}(s')}{\Omega^I_2(s')(s')^3(s'-4m_\pi^2)(s'-s)}\,ds' + \frac{s}{\pi}\int_{4m_\pi^2}^{\infty}\frac{\sin\delta^I_2(s')\,\bar{h}^{I,\mathrm{Born}}_{2,++}(s')}{|\Omega^I_2(s')|(s')^3(s'-4m_\pi^2)(s'-s)}\,ds'\right] \quad (29)$$

and

$$h^I_{2,+-}(s) = \bar{h}^{I,\mathrm{Born}}_{2,+-}(s) + \Omega^I_2(s)s\big(s-4m_\pi^2\big) \times\left[d^{(I)} + \frac{s}{\pi}\int_{-\infty}^{-s_0}\frac{\mathrm{Im}\,\bar{h}^{I,\mathrm{Res}}_{2,+-}(s')}{\Omega^I_2(s')(s')^2(s'-4m_\pi^2)(s'-s)}\,ds' + \frac{s}{\pi}\int_{4m_\pi^2}^{\infty}\frac{\sin\delta^I_2(s')\bar{h}^{I,\mathrm{Born}}_{2,+-}(s')}{|\Omega^I_2(s')|(s')^2(s'-4m_\pi^2)(s'-s)}\,ds'\right]. \quad (30)$$

These representations involve four subtraction constants $c^{(I)}$ and $d^{(I)}$.

Let us finally remark that polynomials can be introduced in MO representations in different ways (for instance multiplying the Omnès functions). It is easy to show that any representation can always be recast in the form given above. These are convenient because the relations between the polynomial coefficients and the pion polarizabilities are now particularly simple.

3.1 Sum rules

Above, we have written over-subtracted dispersion relations in order to suppress the contributions from large values of $|s'|$ in the integrands. Such representations can be valid only in a finite energy domain since, in general, they lead to diverging amplitudes[3] when $s\to\infty$. A priori, the exact asymptotic behavior of the partial-wave amplitudes is not known, but S-matrix unitarity provides the following bound:

$$\big|h^I_{J,\lambda\lambda'}(s)\big| \le \frac{16\pi}{\sqrt{\beta_\pi(s)}} \quad (31)$$

which implies that one could write representations with fewer subtraction constants if one assumes that the integrands are known sufficiently well. This amounts to expressing some of the subtraction constants as sum rules. Such sum rules are very simply obtained from the representations written above by requiring that the most singular terms as $s\to\infty$ are cancelled. For example, the D-wave constants $c^{(I)}$, $d^{(I)}$ get expressed as

$$c^{(I)}\big|_{\mathrm{SR}} = L^{(I)}_{3,++} + R^{(I)}_{3,++},\qquad d^{(I)}\big|_{\mathrm{SR}} = L^{(I)}_{2,+-} + R^{(I)}_{2,+-} \quad (32)$$

with

$$L^{(I)}_{n,\lambda\lambda'} = \frac{1}{\pi}\int_{-\infty}^{-s_0}\frac{\mathrm{Im}\,\bar{h}^{I,\mathrm{Res}}_{2,\lambda\lambda'}(s')}{\Omega^I_2(s')(s')^n(s'-4m_\pi^2)}\,ds',\qquad R^{(I)}_{n,\lambda\lambda'} = \frac{1}{\pi}\int_{4m_\pi^2}^{\infty}\frac{\sin\delta^I_2(s')\bar{h}^{I,\mathrm{Born}}_{2,\lambda\lambda'}(s')}{|\Omega^I_2(s')|(s')^n(s'-4m_\pi^2)}\,ds'. \quad (33)$$

A useful test (which we will perform) of the validity of the integrands, in particular of the modeling of the left-hand cut, is to verify that the values of the subtraction constants obtained from such sum rules are not significantly different from those obtained from fitting to the experimental data.

4 Left-hand cut

In order to proceed with the previous formulas we need to specify the left-hand cut pieces of the $\gamma\gamma\to\pi\pi$ amplitudes (as well as the analogous contributions to $\gamma\gamma\to K\bar{K}$ in the case $I=0$, $J=0$). Quite generally, the left-hand cut can be associated with singularities in the crossed-channel (i.e. $\gamma\pi\to\gamma\pi$) partial waves. A derivation based on the Mandelstam double-spectral representation can be found in ref. [18]. The first cross-channel singularity is the pion pole, followed by the unitarity cuts due to 2π, 3π etc. Here, the pion pole contribution will be exactly taken into account. The discontinuities $\rho_{n\pi}(s)$ associated with the unitarity cuts are calculable from ChPT at small s, but they are strongly suppressed in this region: $\rho_{3\pi}$ has chiral order p^6 while $\rho_{2\pi}$ is even more suppressed and has chiral order p^8. Here, due to the lack of detailed experimental information on the $\gamma\pi\to\gamma\pi$ partial waves, we will content ourselves with simple resonance approximations.

4.1 QED Born amplitudes

Let us first consider the QED Born term contribution to $\gamma\gamma\to\pi^+\pi^-$ (and $\gamma\gamma\to K^+K^-$). The standard result for the helicity amplitudes reads

$$H^{c,\mathrm{Born}}_{++} = \frac{2sm_\pi^2}{(t-m_\pi^2)(u-m_\pi^2)},\qquad H^{c,\mathrm{Born}}_{+-} = \frac{2(tu-m_\pi^4)}{(t-m_\pi^2)(u-m_\pi^2)}. \quad (34)$$

[3] The asymptotic conditions implemented in the T matrices imply that the $I=0$ and $I=2$ Omnès functions behave respectively as s^{-1} and s^0 at large s.

The corresponding Born amplitudes for $\gamma\gamma \to K^+K^-$ are, of course, the same, with m_π replaced by m_K. Performing the partial-wave projection according to (14), one obtains for $J=0$ and $J=2$,

$$\begin{aligned}
\bar{h}^{c,\mathrm{Born}}_{0,++}(s) &= \frac{4m_\pi^2}{s} L_\pi(s),\\
\bar{h}^{c,\mathrm{Born}}_{2,++}(s) &= -\frac{2m_\pi^2}{s}\left[\left(1-\frac{3}{\beta_\pi^2(s)}\right)L_\pi(s)+\frac{6}{\beta_\pi^2(s)}\right],\\
\bar{h}^{c,\mathrm{Born}}_{2,+-}(s) &= \frac{\sqrt{6}}{4}\left[\left(1-\frac{1}{\beta_\pi^2(s)}\right)^2\beta_\pi^2(s)L_\pi(s)\right.\\
&\quad\left.-\frac{2}{\beta_\pi^2(s)}+\frac{10}{3}\right]
\end{aligned} \tag{35}$$

with

$$L_\pi(s) = \frac{1}{\beta_\pi(s)}\log\frac{1+\beta_\pi(s)}{1-\beta_\pi(s)}. \tag{36}$$

We will also need the $J=0$ partial-wave amplitude for $\gamma\gamma \to K^+K^-$ which, as a result of the normalization (14) reads

$$\bar{k}^{c,\mathrm{Born}}_{0,++}(s) = \frac{4\sqrt{2}m_K^2}{s} L_K(s), \tag{37}$$

and the isospin $I=0$ and $I=2$ projections which are easily deduced from (4), (5).

4.2 Resonance contributions

Let us review below the modeling of the left-hand cut as a sum of resonance pole contributions. Resonances which can contribute must have spin larger than or equal to 1. We will consider vector, axial-vector, tensor and axial-tensor contributions. We start by determining the form of the amplitudes and the relation of the coupling constants to the radiative decay widths. We will then discuss the phenomenological determination of the coupling constants.

• Vector resonances

We can start with a Lagrangian coupling a vector meson V a pseudo-scalar meson P (a pion or a Kaon) and a photon field of the form,

$$\mathcal{L}_{VP\gamma} = eC_V\epsilon^{\mu\nu\alpha\beta}F_{\mu\nu}\partial_\alpha P V_\beta. \tag{38}$$

After a small calculation we reproduce the result first obtained by Ko [43],

$$\begin{aligned}
W_V^{\mu\nu} &= \frac{\tilde{C}_V}{m_V^2-t}\left[\left(s-4m_P^2-4t\right)T_1^{\mu\nu}+\frac{1}{2}T_2^{\mu\nu}\right]\\
&\quad+(t\leftrightarrow u),\quad \tilde{C}_V=\frac{1}{2}C_V^2.
\end{aligned} \tag{39}$$

The relation between the coupling $\tilde{C}_V$ and the decay width of the resonance reads,

$$\Gamma_{V\to P\gamma} = \alpha\tilde{C}_V\frac{(m_V^2-m_P^2)^3}{3m_V^3}. \tag{40}$$

Performing the partial-wave projections of these amplitudes one finds for $J=0$ and $J=2$

$$\begin{aligned}
\bar{h}^V_{0,++}(s) &= 4\tilde{C}_V\left[-\frac{m_V^2}{\beta_\pi(s)}L_V(s)+s\right],\\
\bar{h}^V_{2,++}(s) &= \tilde{C}_V\frac{2m_V^2}{\beta_\pi(s)}\left[\left(1-3X_V^2(s)\right)L_V(s)+6X_V(s)\right],\\
\bar{h}^V_{2,+-}(s) &= \tilde{C}_V\frac{\sqrt{6}}{4}s\beta_\pi(s)\left[\left(1-X_V^2(s)\right)^2L_V(s)\right.\\
&\quad\left.+\frac{2}{3}X_V(s)\left(5-3X_V^2(s)\right)\right]
\end{aligned} \tag{41}$$

where the logarithmic function L_V reads

$$\begin{aligned}
L_V(s) &= \log\frac{X_V(s)+1}{X_V(s)-1},\\
X_V(s) &= \frac{2m_V^2-2m_\pi^2+s}{s\beta_\pi(s)}.
\end{aligned} \tag{42}$$

One remarks here that a term linear in s appears in the expression for the amplitude $\bar{h}^V_{0,++}$. This is an illustration of possible polynomial ambiguities. Indeed, if one uses an antisymmetric tensor description of a vector particle (e.g. [44]) this term would appear with the opposite sign. In the modified MO representation we need only the imaginary parts of the partial-wave amplitudes along the cut, which are free of any ambiguity. The left-hand cut is contained in the function $L_V(s)$. Rewriting X_V as

$$\begin{aligned}
X_V^2(s) &= 1+\frac{4m_V^2(s+s_V)}{s(s-4m_\pi^2)},\\
s_V &= \frac{(m_V^2-m_\pi^2)^2}{m_V^2}
\end{aligned} \tag{43}$$

one deduces that the cut extends from $-\infty$ to $-s_V$. One then derives the imaginary parts of the amplitudes

$$\begin{aligned}
\frac{1}{\pi}\operatorname{Im}\bar{h}^V_{0,++}(s) &= -4\tilde{C}_V\frac{m_V^2}{\beta_\pi(s)}\theta(-s-s_V),\\
\frac{1}{\pi}\operatorname{Im}\bar{h}^V_{2,++}(s) &= -2\tilde{C}_V\frac{m_V^2}{\beta_\pi(s)}\left(3X_V^2(s)-1\right)\theta(-s-s_V),\\
\frac{1}{\pi}\operatorname{Im}\bar{h}^V_{2,+-}(s) &= \frac{\sqrt{6}}{4}\tilde{C}_V s\beta_\pi(s)\left(X_V^2(s)-1\right)^2\theta(-s-s_V).
\end{aligned} \tag{44}$$

We remark that the sharp cutoff $\theta(-s-s_V)$ which appears in the imaginary parts is associated with the narrow width approximation. Introducing a finite width smooths the cut-off in the region $s=-s_V$. The corresponding contributions to $\gamma\gamma\to K\bar{K}$ partial-wave amplitudes (i.e. $\bar{k}^V_{0,++}$, $\bar{k}^V_{2,++}$ $\bar{k}^V_{0,+-}$) are obtained by replacing in (41) m_π by m_K and $\tilde{C}_V$ by $\sqrt{2}\tilde{C}_V$ (in accordance with the normalizations defined in (14)).

• Axial-vector resonances

We will designate generically the C-odd axial-vectors as B and the C-even ones by A. The following Lagrangian describes $B\to P\gamma$ coupling:

$$\mathcal{L}_{B\to P\gamma}=eC_B F_{\mu\nu}\partial^\mu B^\nu P, \tag{45}$$

from which we easily deduce the amplitude $\gamma\gamma\to PP$ amplitude corresponding to B exchange,

$$W_B^{\mu\nu}=\frac{\tilde{C}_B}{m_A^2-t}\left[\left(s-4m_P^2+4t\right)T_1^{\mu\nu}+\frac{1}{2}T_2^{\mu\nu}\right] + (t\leftrightarrow u),\quad \tilde{C}_B=\frac{1}{8}C_B^2. \tag{46}$$

As before, the couplings $\tilde{C}_B$ must be deduced from experimental data on $B\to P\gamma$ decay using

$$\Gamma_{B\to P\gamma}=\alpha\tilde{C}_B\frac{(m_B^2-m_P^2)^3}{3m_B^3}. \tag{47}$$

Working out the helicity amplitudes corresponding to (46), one sees that they are simply related to the helicity amplitudes associated with vector resonances:

$$\begin{aligned}&H^B_{++}(\tilde{C}_B,m_B,s,t)=-H^V_{++}(\tilde{C}_V\to\tilde{C}_B,m_V\to m_B,s,t),\\&H^B_{+-}(\tilde{C}_B,m_B,s,t)=H^V_{+-}(\tilde{C}_V\to\tilde{C}_B,m_V\to m_B,s,t)\end{aligned} \tag{48}$$

from which one easily deduces the imaginary parts of the partial-wave projections from (44).

• Tensor resonances

The Lagrangian coupling a tensor meson (quantum numbers 2^{++}) to a photon and a pseudo-scalar meson must have the following form:

$$\mathcal{L}_{TP\gamma}=eC_T\epsilon^{\mu\nu\alpha\beta}F_{\mu\nu}T^\lambda_\alpha\partial_\lambda\partial_\beta P. \tag{49}$$

From this, we can first deduce the relation between the decay width and the coupling constant

$$\Gamma_{T\to P\gamma}=\alpha\tilde{C}_T\frac{(m_T^2-m_P^2)^5}{5m_T^5},\quad \tilde{C}_T=\frac{C_T^2}{16}. \tag{50}$$

After a small calculation we can obtain the form of the $\gamma\gamma\to PP$ amplitude generated by tensor meson exchange

$$W_T^{\mu\nu}=A_T(s,t)T_1^{\mu\nu}+B_T(s,t)T_2^{\mu\nu}+(t\leftrightarrow u) \tag{51}$$

with

$$\begin{aligned}B_T(s,t)&=\frac{\tilde{C}_T[(t+m_\pi^2)^2+4m_T^2(s-m_\pi^2)]}{2m_T^2(m_T^2-t)},\\A_T(s,t)&=2\left(s-4m_\pi^2-4t\right)B_T(s,t)-\frac{8\tilde{C}_T(t-m_\pi^2)^2}{m_T^2-t}.\end{aligned} \tag{52}$$

From here, we can construct the helicity amplitudes and their projections. We quote below the imaginary parts of these along the left-hand cut

$$\begin{aligned}\frac{1}{\pi}\operatorname{Im}\bar{h}^T_{0,++}(s)&=-4\tilde{C}_T\frac{m_T^2}{\beta_\pi(s)}[4s+3s_T]\theta(-s-s_T),\\\frac{1}{\pi}\operatorname{Im}\bar{h}^T_{2,++}(s)&=-2\tilde{C}_T\frac{m_T^2}{\beta_\pi(s)}\left(3X_T^2(s)-1\right)\\&\quad\times[4s+3s_T]\theta(-s-s_T),\\\frac{1}{\pi}\operatorname{Im}\bar{h}^T_{2,+-}(s)&=\frac{\sqrt{6}}{4}\tilde{C}_T s\beta_\pi(s)\left(X_T^2(s)-1\right)^2\\&\quad\times[4s+s_T)]\theta(-s-s_T).\end{aligned} \tag{53}$$

• Axial-tensor resonances

For illustrative purposes, finally, let us consider axial-tensor (i.e. with quantum number $J^P=2^-$) resonances. The relevant Lagrangian has the following form:

$$\mathcal{L}_{T_AP\gamma}=eC_{T_A}F_{\mu\nu}T_A^{\nu\lambda}\partial_\mu\partial_\lambda P \tag{54}$$

and we deduce the following relation with the radiative decay width:

$$\Gamma_{T_A\to P\gamma}=\alpha\tilde{C}_{T_A}\frac{(m_{T_A}^2-m_P^2)^5}{5m_{T_A}^5},\quad \tilde{C}_{T_A}=\frac{C_{T_A}^2}{64}. \tag{55}$$

Next, one computes the diagrams contributing to $\gamma\gamma\to PP$ and one finds the result

$$\begin{aligned}B_{T_A}(s,t)&=\frac{\tilde{C}_{T_A}[(t+m_\pi^2)^2+4m_{T_A}^2(s-m_\pi^2)]}{2m_{T_A}^2(m_{T_A}^2-t)},\\A_{T_A}(s,t)&=2\left(s-4m_\pi^2+4t\right)B_{T_A}(s,t)\\&\quad+\frac{8\tilde{C}_{T_A}(t-m_\pi^2)}{(m_{T_A}^2-t)}.\end{aligned} \tag{56}$$

Constructing the helicity amplitudes, one notices the following simple relations between the tensor and the axial-tensor

amplitudes:

$$
\begin{aligned}
&H^{T_A}_{++}(\tilde{C}_{T_A}, m_{T_A}, s, t) \\
&\quad = -H^{T}_{++}(\tilde{C}_T \to \tilde{C}_{T_A}, m_T \to m_{T_A}, s, t), \\
&H^{T_A}_{+-}(\tilde{C}_{T_A}, m_{T_A}, s, t) \\
&\quad = H^{T}_{+-}(\tilde{C}_T \to \tilde{C}_{T_A}, m_T \to m_{T_A}, s, t).
\end{aligned}
\tag{57}
$$

Alternative expressions can be derived for the resonance exchanges, which are somewhat more transparent physically and easier to generalize to arbitrary spin S. They involve rotation functions $d^S_{\lambda,\lambda'}(z_R)$ where z_R is the center-of-mass scattering angle for the crossed-channel amplitude $\gamma\pi \to \gamma\pi$ at the resonance mass,

$$
z_R = 1 + \frac{2st}{(t-m_\pi^2)^2}\bigg|_{t=m_R^2} = 1 + \frac{2s}{s_R} \tag{58}
$$

(using (43)) and generalized Legendre polynomials $P^m_J(X_R)$. The vector-exchange partial-wave helicity amplitudes can be expressed as

$$
\begin{aligned}
\frac{1}{\pi}\operatorname{Im}\bar{h}^V_{0,++}(s) &= -4\tilde{C}_V \frac{m_V^2 s_V}{\sqrt{s(s-4m_\pi^2)}} P^0_0(X_V) \\
&\quad \times d^1_{1,-1}(z_V)\theta(-s-s_V), \\
\frac{1}{\pi}\operatorname{Im}\bar{h}^V_{2,++}(s) &= -4\tilde{C}_V \frac{m_V^2 s_V}{\sqrt{s(s-4m_\pi^2)}} P^0_2(X_V) \\
&\quad \times d^1_{1,-1}(z_V)\theta(-s-s_V), \\
\frac{1}{\pi}\operatorname{Im}\bar{h}^V_{2,+-}(s) &= -\frac{\sqrt{6}}{3}\tilde{C}_V \frac{m_V^2 s_V}{\sqrt{s(s-4m_\pi^2)}} P^2_2(X_V) \\
&\quad \times d^1_{1,1}(z_V)\theta(-s-s_V).
\end{aligned}
\tag{59}
$$

Analogously, the tensor exchange amplitudes involve the rotation functions $d^2_{\lambda,\lambda'}(z_T)$

$$
\begin{aligned}
\frac{1}{\pi}\operatorname{Im}\bar{h}^T_{0,++}(s) &= -4\tilde{C}_T \frac{m_T^2 s_T^2}{\sqrt{s(s-4m_\pi^2)}} P^0_0(X_T) \\
&\quad \times d^2_{1,-1}(z_T)\theta(-s-s_T), \\
\frac{1}{\pi}\operatorname{Im}\bar{h}^T_{2,++}(s) &= -4\tilde{C}_T \frac{m_T^2 s_T^2}{\sqrt{s(s-4m_\pi^2)}} P^0_2(X_T) \\
&\quad \times d^2_{1,-1}(z_T)\theta(-s-s_T), \\
\frac{1}{\pi}\operatorname{Im}\bar{h}^T_{2,+-}(s) &= -\frac{\sqrt{6}}{3}\tilde{C}_T \frac{m_T^2 s_T^2}{\sqrt{s(s-4m_\pi^2)}} P^2_2(X_T) \\
&\quad \times d^2_{1,1}(z_T)\theta(-s-s_T).
\end{aligned}
\tag{60}
$$

From these expressions, it is easy to guess the form of the amplitudes for an arbitrary angular momentum J, or generated by the exchange of a meson of arbitrary spin S. Because of the polynomial functions $d^S_{\lambda,\lambda'}(1+2s/s_R)$, the behavior of the amplitudes as a function of s becomes worse as the spin S of the exchanged resonance increases. As usual, one expects that a Regge-type regularization will occur upon including an infinite set of resonances. In practice, one can simulate this by introducing a cutoff on the left-cut integration.

Table 1 Signs of the imaginary parts of the helicity amplitudes as generated from various resonance exchanges

$\lambda\lambda'$	V	A	T	T_A
$++$	$-$	$+$	$+$	$-$
$+-$	$-$	$-$	$+$	$+$

Let us make a remark on the signs of these resonance amplitudes. Varying s from $-\infty$ to $-s_R$, the quantity $X_R(s)$ varies from -1 to 1. The Legendre polynomial $P_2(X_R)$ passes through a zero, implying that $\operatorname{Im}\bar{h}^R_{2,++}$ changes sign while the amplitudes $\operatorname{Im}\bar{h}^R_{2,+-}$ and $\operatorname{Im}\bar{h}^R_{0,++}$ do not. This feature partly explains why, upon integration over s, the $+-$ D-wave amplitude is larger than the $++$ one. Furthermore, there are alternating signs between the various resonance contributions: see Table 1. The table illustrates that the signs corresponding to a spin S and a spin $S+1$ resonance are opposite (this can be shown to be true for arbitrary S). Furthermore, for the $++$ amplitudes, the signs alternate between C-even and C-odd resonance contributions. The resulting behavior of some of the integrands from which the left-cut functions are computed is illustrated in Fig. 2. This figure illustrates the numerical importance of the tensor contribution in the helicity $+-$ amplitude.

4.3 Phenomenological determination of the coupling constants:

• Neutral resonances

The neutral resonances which can decay into a photon and a π^0 must be odd under charge conjugation. This is the case of the vector mesons ρ^0, ω and their properties are rather well known experimentally. The results from the PDG [42] and the corresponding values of the couplings $\tilde{C}_V$ are collected in Table 2 below including also the result for the $K^{*0}(892)$.

The experimental information concerning the C-odd axial meson radiative decays is not as detailed as in the case of the vector mesons. The PDG quotes a result for $b_1^+(1235)$ decay: $\Gamma(b_1^+(1235) \to \pi^+\gamma) = 240 \pm 60$ KeV, whereas the corresponding radiative widths of the neutral axials $b_1^0(1235)$ and $h_1(1170)$ have not yet been measured. A rough estimate of these, using nonet symmetry, is:

$$
\tilde{C}_{b_1^0(1235)} \simeq \tilde{C}_{b_1^+(1235)}, \qquad \tilde{C}_{h_1^0(1170)} \simeq 9\tilde{C}_{b_1^+(1235)}. \tag{61}
$$

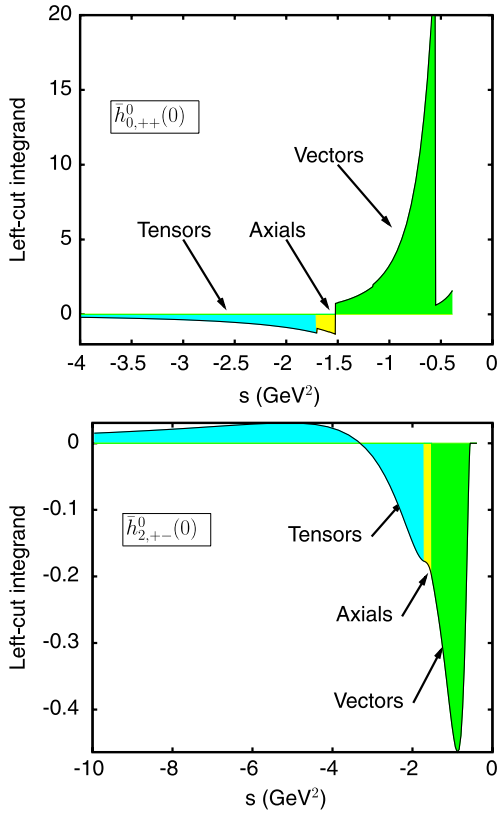

Fig. 2 Left-cut integrand for $h^0_{0,++}(0)$ (*upper figure*, see (23)) and $h^0_{2,+-}(0)$ (*lower figure*, see (30)) illustrating the role of the various contributing resonances

Table 2 Radiative widths of neutral vector mesons and of neutral C-odd axial-vector mesons from the PDG [42] and the corresponding couplings $\tilde{C}_R$

	Γ (keV)	$\tilde{C}_R$ (GeV^{-2})
$\omega \to \pi^0\gamma$	703 ± 25	0.66 ± 0.023
$\rho^0 \to \pi^0\gamma$	89 ± 12	0.09 ± 0.01
$\phi \to \pi^0\gamma$	5.4 ± 0.5	$(0.2 \pm 0.02)10^{-2}$
$K^{*0} \to K^0\gamma$	117 ± 10	0.20 ± 0.02
$h_1(1170) \to \pi^0\gamma$	–	$\simeq 0.45$
$b_1(1235) \to \pi^0\gamma$	–	$\simeq 0.05$
$K_1(1270) \to K^0\gamma$	73 ± 29	0.024 ± 0.010
$K_1(1400) \to K^0\gamma$	280 ± 46	0.063 ± 0.010

Concerning the strange axials, we can use here the experimental results on the radiative decays of the neutral $K_1(1270)$, $K_1(1400)$ which can be found in the PDG. We collect this information and the results for the $\tilde{C}_B$ couplings in the lower part of Table 2. Finally, both C-odd and C-even axial-tensor mesons are expected to exist in the quark model with a mass around 1.7 GeV [45]. Experimentally, the C-even axial-tensor meson $\pi_2(1670)$ is mentioned in the PDG, but not the C-odd. The decay width of the $\pi_2(1670)$ into $\gamma\pi$ is not known.

Table 3 Same as Table 2 for charged vectors, axial-vectors and tensor resonances

	Γ (keV)	$\tilde{C}_R$ (GeV^{-2})
$\rho^+ \to \pi^+\gamma$	68 ± 7	0.066 ± 0.007
$K^{*+} \to K^+\gamma$	50 ± 5	0.085 ± 0.009
$a_1^+(1260) \to \pi^+\gamma$	640 ± 240	0.15 ± 0.06
$b_1^+(1235) \to \pi^+\gamma$	230 ± 60	0.05 ± 0.01
$K_1^+(1270) \to K^+\gamma$	–	$\simeq 0.20$
$K_1^+(1400) \to K^+\gamma$	–	$\simeq 0.00$
$a_2^+(1320) \to \pi^+\gamma$	287 ± 30	0.052 ± 0.005
$K_2^{*+}(1430) \to K^+\gamma$	241 ± 50	0.053 ± 0.011

• **Charged resonances**

Here, we can have contributions from vector mesons $\rho^+(770)$, $K^{*+}(892)$ and from C-odd and C-even axial-vector mesons $a_1^+(1260)$, $b_1^+(1235)$, $K_1^+(1270)$, $K_1^+(1400)$. We have also considered the contributions from the tensor mesons $a_2^+(1320)$, $K_2^{*+}(1430)$ since their masses are comparable to those of the axial-vectors. The relevant couplings $\tilde{C}_V$ for the vector mesons in the charged case can be deduced from experiment and are collected in Table 3. In the case of the axial-vectors, results are available for the $b_1^+(1235)$ [46] as well as for the $a_1^+(1260)$ [47] from Primakoff experiments. We must however keep in mind that results from photoproduction experiments [48, 49] suggest that the radiative width of the $a_1^+(1260)$ could actually be smaller than claimed in [47]. Concerning the charged strange axials, $K_1(1270)$, $K_1(1400)$, unfortunately, no experimental information is available on their radiative widths. Rough estimates can again be made using nonet symmetry, which leads to the following relations:

$$\begin{aligned} &\tilde{C}_{K_1^0(1270)} + \tilde{C}_{K_1^0(1400)} = 4\tilde{C}_{b_1^+(1235)}, \\ &\tilde{C}_{K_1^+(1270)} + \tilde{C}_{K_1^+(1400)} = \tilde{C}_{b_1^+(1235)} + \tilde{C}_{a_1^+(1260)}. \end{aligned} \tag{62}$$

The first relation is obeyed by the experimental results within a factor of two. In order to determine the couplings $\tilde{C}_{K_1^+(1270)}$ and $\tilde{C}_{K_1^+(1400)}$ separately we note that one of them should be enhanced relative to the other by the Lipkin mechanism [50]. It seems plausible that it should be $\tilde{C}_{K_1^+(1270)}$ because its main decay mode is via $K^+\rho^0$ which can produce $K^+\gamma$ via vector meson dominance.

5 Pion polarizabilities and chiral symmetry constraints

5.1 Polarizabilities

Polarizabilities are important observables which probe the structure of the pion. Using crossing symmetry and analyticity one can relate the amplitudes $\gamma\gamma \to \pi^+\pi^-$, $\pi^0\pi^0$ at $t = m_\pi^2$ and small s to the electric and magnetic polarizabilities of the charged and the neutral pion respectively. These pionic observables have been computed in Chiral perturbation theory at next to leading order [24, 25] and then at next-to-next to leading order [51–54]. Some of these results which are relevant to our analysis will be recalled in the next subsection. There are simple relations between the subtraction constants introduced in the dispersive relations for the partial waves and the electric/magnetic polarizabilities of the pion. From the partial waves with $J = 0$ and $J = 2$ which are involved in our analysis we can access the dipole and the quadrupole polarizabilities. We list below the relevant formulas. The polarizabilities of the neutral pion are defined as follows from the expansions of H^n_{++} and H^n_{+-} around $s = 0$, $t = m_\pi^2$ (see e.g. [53]):

$$\begin{aligned}
&\frac{2\alpha}{m_\pi}\frac{H^n_{++}(s,t=m_\pi^2)}{s} \\
&\quad = (\alpha_1-\beta_1)_{\pi^0} + \frac{s}{12}(\alpha_2-\beta_2)_{\pi^0} + \cdots, \\
&\frac{-2\alpha}{m_\pi}\frac{H^n_{+-}(s,t=m_\pi^2)}{s} \\
&\quad = (\alpha_1+\beta_1)_{\pi^0} + \frac{s}{12}(\alpha_2+\beta_2)_{\pi^0} + \cdots
\end{aligned} \tag{63}$$

(the minus sign in from of H^n_{+-} is associated with our choice for the photon polarization vectors). The charged pion polarizabilities are defined by the expansion of the amplitudes after removing the Born term, i.e. defining $\hat{H}^c_{\lambda\lambda'} = H^c_{\lambda\lambda'} - H^{c,\mathrm{Born}}_{\lambda\lambda'}$,

$$\begin{aligned}
&\frac{2\alpha}{m_\pi}\frac{\hat{H}^c_{++}(s,t=m_\pi^2)}{s} \\
&\quad = (\alpha_1-\beta_1)_{\pi^+} + \frac{s}{12}(\alpha_2-\beta_2)_{\pi^+} + \cdots, \\
&\frac{-2\alpha}{m_\pi}\frac{\hat{H}^c_{+-}(s,t=m_\pi^2)}{s} \\
&\quad = (\alpha_1+\beta_1)_{\pi^+} + \frac{s}{12}(\alpha_2+\beta_2)_{\pi^+} + \cdots.
\end{aligned} \tag{64}$$

Performing the partial-wave expansion, the $J = 0$ and $J = 2$ partial waves are the only ones which contribute to the dipole and quadrupole polarizabilities.

The polarizabilities are simply related to the subtraction constants in the dispersive representations. Comparing with those (23) (26) for $h^0_{0,++}$ and $h^2_{0,++}$ we obtain for the polarizability differences

$$\begin{aligned}
(\alpha_1-\beta_1)_{\pi^+} &= -\frac{1}{\sqrt{6}}\frac{2\alpha}{m_\pi}\big(\sqrt{2}b^{(0)} + b^{(2)}\big), \\
(\alpha_1-\beta_1)_{\pi^0} &= -\frac{1}{\sqrt{3}}\frac{2\alpha}{m_\pi}\big(b^{(0)} - \sqrt{2}b^{(2)}\big).
\end{aligned} \tag{65}$$

Similarly, the polarizability sums are obtained from the subtraction constants d^I which appear in the $J = 2$ spin-flip amplitudes $h^I_{2,+-}$ (see (29), (30))

$$\begin{aligned}
(\alpha_1+\beta_1)_{\pi^+} &= -10\alpha m_\pi\big(\sqrt{2}d^{(0)} + d^{(2)}\big), \\
(\alpha_1+\beta_1)_{\pi^0} &= -10\sqrt{2}\alpha m_\pi\big(d^{(0)} - \sqrt{2}d^{(2)}\big).
\end{aligned} \tag{66}$$

Considering the quadrupole polarizabilities now, we list below the polarizabilities defined for $I = 0$ and $I = 2$ amplitudes which can be easily combined using (4). For the polarizability differences, we get

$$\begin{aligned}
(\alpha_2-\beta_2)^{(0)} =& \frac{24\alpha}{m_\pi}\big(\dot{\Omega}_{11}b^{(0)} + \dot{\Omega}_{12}b_K^{(0)} + b'^{(0)} \\
&+ 10m_\pi^2 c^{(0)}\big), \\
(\alpha_2-\beta_2)^{(2)} =& \frac{24\alpha}{m_\pi}\big(\dot{\Omega}_0^2\, b^{(2)} + b'^{(2)} + 10\,m_\pi^2 c^{(2)}\big).
\end{aligned} \tag{67}$$

For the sum of the quadrupole polarizabilities, we get

$$\begin{aligned}
(\alpha_2+\beta_2)^{(0)} &= 120\sqrt{6}m_\pi\alpha\big(\dot{\Omega}_2^0 d^{(0)} + d'^{(0)}\big), \\
(\alpha_2+\beta_2)^{(2)} &= 120\sqrt{6}m_\pi\alpha\big(\dot{\Omega}_2^2 d^{(2)} + d'^{(2)}\big).
\end{aligned} \tag{68}$$

In these formulas the derivatives of the Omnès functions at $s = 0$ appear, denoted by, e.g. $\dot{\Omega}_{11}$. In (68) the quantities $d'^{(0)}$, $d'^{(2)}$ are given by sum rules:

$$d'^{(I)} = L^{(I)}_{3,+-} + R^{(I)}_{3,+-} \tag{69}$$

where the integrals are defined in (33). Finally, the subtraction parameter $b_K^{(0)}$ which appears in the analysis through coupled channel unitarity is related to the $I = 0$ kaon polarizability as follows:

$$(\alpha_1-\beta_1)^{(0)}_K = \frac{\sqrt{2}\alpha}{m_K}b_K^{(0)}. \tag{70}$$

5.2 Constraints from chiral symmetry

Chiral symmetry constrains the amplitudes $\gamma\gamma \to \pi^0\pi^0$, $\pi^+\pi^-$ for small values of the Mandelstam variables s, t. Computations up to NNLO in the chiral expansion have been performed [51–54]. At this order, the amplitudes involve 13 coupling constants from the $O(p^6)$ chiral Lagrangian. More precisely, three combinations of such couplings are involved which we will denote a_1^r, a_2^r, b^r for $\pi^0\pi^0$

and $\tilde{a}_1^r$, $\tilde{a}_2^r$, $\tilde{b}^r$ for $\pi^+\pi^-$. Most of the $O(p^6)$ couplings are as yet undetermined, but in the case of $\pi^0\pi^0$ we can make use of a chiral sum rule for one coupling. We explain this below. We also recall the chiral expressions for the pion polarizabilities which allows one to assess which chiral constraints can be used in the fits to the experimental data.

(a) $\pi^0\pi^0$:

The dipole polarizabilities of the neutral pion have the following expressions in ChPT, in terms of the coupling combinations a_1^r, a_2^r, b^r:

$$(\alpha_1-\beta_1)_{\pi_0} = \frac{\alpha}{16\pi^2 F_\pi^2 m_\pi}\Bigg[-\frac{1}{3} + \frac{m_\pi^2}{16\pi^2 F_\pi^2}\big(a_1^r + 8b^r + X_{1-}(\mu)\big)\Bigg], \tag{71}$$
$$(\alpha_1+\beta_1)_{\pi_0} = \frac{\alpha m_\pi}{(16\pi^2 F_\pi^2)^2}\big[8b^r + X_{1+}(\mu)\big]$$

where the quantities $X_{1-}(\mu)$, $X_{1+}(\mu)$ involve chiral logarithms and known $O(p^4)$ couplings. Their detailed expressions can be found in Ref. [53]. The chiral expressions for the quadrupole polarizabilities read

$$(\alpha_2-\beta_2)_{\pi_0} = \frac{\alpha}{16\pi^2 F_\pi^2 m_\pi^3}\Bigg[\frac{156}{45} + \frac{m_\pi^2}{16\pi^2 F_\pi^2}\big(12\big(a_2^r - 2b^r\big) + X_{2-}(\mu)\big)\Bigg], \tag{72}$$
$$(\alpha_2+\beta_2)_{\pi_0} = \frac{\alpha}{(16\pi^2 F_\pi^2)^2 m_\pi}\Bigg[-\frac{5009}{27} + \frac{13435\pi^2}{720} + \frac{16}{45}\bar{l}_2\Bigg].$$

Based on resonance model estimates for the $O(p^6)$ couplings, numerical values for the polarizability differences at $O(p^6)$ were obtained [53]. We display them below together with the $O(p^4)$ values, which illustrates that $O(p^6)$ effects can be rather large for these observables:

$$\begin{array}{lll} & O(p^4) & O(p^6) \\ (\alpha_1-\beta_1)_{\pi_0} = & -1.0, & -1.9\ (10^{-4}\ \mathrm{fm}^3) \\ (\alpha_2-\beta_2)_{\pi_0} = & 20.7, & 37.6\ (10^{-4}\ \mathrm{fm}^5). \end{array} \tag{73}$$

The reliability of naive resonance saturation models has not been established for $O(p^6)$ couplings. Here, we will only make use of a model independent estimate for the single coupling c_{34}^r. This estimate is based on a chiral sum rule [55, 56] associated with differences of correlators of two vector currents: $\langle V^3V^3 - V^8V^8\rangle$ or $\langle V^{ud}V^{du} - V^{us}V^{su}\rangle$, from which the $SU(3)$ coupling C_{61}^r can be determined. Using three-flavor ChPT and matching to two-flavor ChPT it can be turned into an evaluation of the coupling c_{34}^r (a simplified version of this sum rule was used earlier in Ref. [57]). Such matching relations have been obtained recently by Gasser et al. [58] for the Lagrangian operators which do not vanish in the limit $m_u = m_d = 0$. We can obtain the matching relation for c_{34}^r by going to this limit after taking a derivative with respect to $m_u + m_d$. Using the $O(p^6)$ ChPT calculations of the $\langle V^3V^3\rangle$ correlator performed in Ref. [59], and taking the derivative with respect to m_π^2 one finds the following matching formula:

$$c_{34}^r = \frac{F^2}{192\times 16\pi^2\bar{m}_K^2} + C_{61}^r + 2C_{62}^r - \frac{1}{4\times 32\pi^2}\Big(\log\frac{\bar{m}_K^2}{\mu^2}+1\Big)\big(L_9^r + L_{10}^r\big) + O\big(\bar{m}_K^2\big) \tag{74}$$

(where $\bar{m}_K^2 = \lim_{m_u=m_d=0} m_K^2$). This relation allows one to evaluate c_{34}^r provided we further invoke a large N_c argument which implies that $C_{62}^r(\mu)$ should be suppressed compared with $C_{61}^r(\mu)$ when $\mu \simeq 1$ GeV. The authors of Ref. [56] have determined that

$$\Pi_{V^3}(0) - \Pi_{V^K}(0) = (1.92\pm 0.27)10^{-2} \tag{75}$$

(using the notations of Ref. [59] for the $\langle VV\rangle$ correlation functions). Using further the explicit chiral formulas from this work [59] and the matching relation (74) above, we find

$$c_{34}^r(\mu = m_\rho) = (1.19\pm 0.43)10^{-5}. \tag{76}$$

Let us note the relation between c_{34}^r and the combinations which appear in the $\pi^0\pi^0$ amplitudes

$$\big(a_1^r + 8b^r\big) + 2\big(a_2^r - 2b^r\big) = 4094\pi^4 c_{34}^r \equiv c_{34}^{\mathrm{eff}}(\mu). \tag{77}$$

In other terms, the combination $6(\alpha_1-\beta_1)_{\pi^0} + m_\pi^2(\alpha_2-\beta_2)_{\pi^0}$ depends on the single $O(p^6)$ coupling, c_{34}. Numerically, using $\mu = m_\rho$ in the ChPT expressions, the following relation is obtained between the dipole and quadrupole polarizabilities:

$$6(\alpha_1-\beta_1)_{\pi^0} + m_{\pi^0}^2(\alpha_2-\beta_2)_{\pi^0} = \big[6.20 + 0.25 c_{34}^{\mathrm{eff}}(m_\rho)\big]10^{-4}\ \mathrm{fm}^3 \tag{78}$$

with $c_{34}^{\mathrm{eff}}(m_\rho) = 4.75\pm 1.71$.

(b) $\pi^+\pi^-$:

In the case of the charged pion, the dipole polarizabilities are given in terms of $\bar{l}_6 - \bar{l}_5$ at $O(p^4)$ and involve three combinations of couplings $\tilde{a}_1^r$, $\tilde{a}_2^r$, $\tilde{b}^r$ at $O(p^6)$

$$(\alpha_1-\beta_1)_{\pi^+} = \frac{\alpha}{16\pi^2 F_\pi^2 m_\pi}\Bigg[\frac{2}{3}(\bar{l}_6 - \bar{l}_5)$$

$$+\frac{m_\pi^2}{16\pi^2F_\pi^2}\big(\tilde{a}_1^r+8\tilde{b}^r+\tilde{X}_{1-}(\mu)\big)\Big],\qquad(79)$$

$$(\alpha_1+\beta_1)_{\pi^+}=\frac{\alpha m_\pi}{(16\pi^2F_\pi^2)^2}\big[8\tilde{b}^r+\tilde{X}_{1+}(\mu)\big].$$

The fully explicit expressions can be found in Refs. [52, 54]. The quadrupole polarizabilities are given as follows:

$$(\alpha_2-\beta_2)_{\pi^+}=\frac{\alpha}{16\pi^2F_\pi^2m_\pi^3}\Big[2+\frac{m_\pi^2}{16\pi^2F_\pi^2}\times\big(12\big(\tilde{a}_2^r-2\tilde{b}^r\big)+\tilde{X}_{2-}(\mu)\big)\Big],$$

$$(\alpha_2+\beta_2)_{\pi^+}=\frac{\alpha}{(16\pi^2F_\pi^2)^2m_\pi}\Big[-\frac{2062}{27}+\frac{10817\pi^2}{1440}+\frac{8}{45}\bar{l}_1+\frac{8}{15}\bar{l}_2\Big].\qquad(80)$$

Unfortunately, for the charged pion, there is no known model independent information[4] on either of the three combinations $\tilde{a}_1^r,\tilde{a}_2^r,\tilde{b}^r$. In this case, we will accept the estimates of Ref. [54] stating that the polarizability difference should lie in the range $(\alpha_1-\beta_1)_{\pi^+}\in[4.70,6.70]\times10^{-4}$ fm^3.

6 Some details on the calculations

6.1 Inputs for the $\pi\pi$ T-matrix

We describe here our inputs for $\pi\pi$ scattering amplitudes which are needed for the S and the D waves. At medium energies $\pi\pi\to\pi\pi$ phase-shifts and inelasticities have been measured in production experiments (see [61] for a review). Considerable progress has been achieved recently in measuring phase-shifts at very low energies as well as the $I=0,2$ S-wave scattering lengths [10–13]. In our analysis, the low-energy region is emphasized in the integrals by the $s=0$ subtractions. Interpolating between the medium- and low-energy regions is controlled by the set of Roy equations [62].

I = 0

Let us consider the S-wave at first. As our main input, we will use the Roy equations results from Ref. [63] for the $I=0$ S-waves in the energy range $E\le0.8$ GeV. In the range $E>0.8$ GeV we perform fits to the experimental results of Ref. [41].[5] Below 1 GeV, we will also make use of the phase-shift determinations of Refs. [66, 67]. These also use the Roy equations as well as other dispersion relations as constraints. The phase-shifts differs from [63] by a few degrees in the matching point region $E\simeq0.8$ GeV: see Fig. 3. The differences in the results will serve us in estimating the errors.

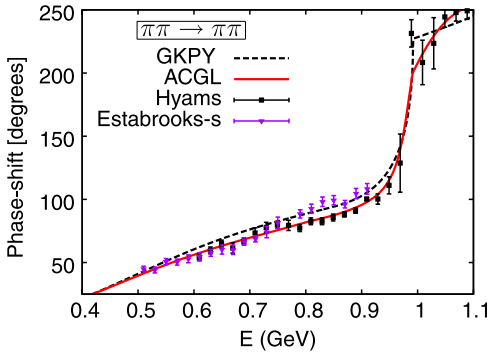

Fig. 3 S-wave $I=0$ $\pi\pi$ phase-shifts below 1 GeV: comparison of two determinations [63, 67] used in our analysis

A well known feature of $\pi\pi$ scattering with $I=J=0$ is the sharp onset of inelasticity when the energy passes the $K\bar{K}$ threshold, which is caused by the $f_0(980)$ resonance. In the energy range which interest us here, it is a good approximation to ignore other inelastic channels and implement exact two-channel unitarity. We can deduce the required T-matrix elements directly from experimental inputs on $\pi\pi\to\pi\pi$ and $\pi\pi\to K\bar{K}$ scattering in the physical region and make use of analyticity in the unphysical region. Also, we work in the isospin limit and assume that this limit can be taken smoothly near the $K\bar{K}$ threshold. Then, the phase of the T-matrix element $T_{12}(s)\equiv g_0^0(s)$ should be equal to the phase of $T_{11}(s)\equiv f_0^0(s)$ (i.e. to the elastic $\pi\pi$ phase-shift) when $\sqrt{s}=2m_K$. This threshold phase is actually not very well known at present: for illustration, the K-matrix fit of Hyams et al. [41] gives $\delta(2m_K)\simeq175°$ while the GKPY [67] analysis gives $\delta(2m_K)\simeq227°$. Concerning T_{12}, the two experiments by Cohen et al. [68] and Etkin et al. [69] are in disagreement close to the threshold, for both the phase and the modulus. The results of Cohen et al. are in accord with a large value of the threshold phase $\delta(2m_K)\simeq220°$ while, on the contrary, Etkin et al. favor a value smaller than 150°. An alternative possibility associated with the results of Etkin et al., is that of a fast variation of the phase in between the $K^0\bar{K}^0$ and the $K^+\bar{K}^-$ thresholds, as suggested in Ref. [70]. In that case, the isospin limit would not be smooth.

In order to probe the sensitivity of the $\gamma\gamma$ data to the value of the threshold phase, we have performed our fits allowing it to vary in the range $150°\le\delta(2m_K)\le220°$. Figure 4 (upper plot) shows our fits of the $\pi\pi\to K\bar{K}$ phase compared to the two data sets. Below the inelastic threshold, in the region 0.8 GeV $\le E\le2m_K$ we adopt the following

[4] A soft pion theorem due to Terazawa [60] has sometimes been applied to the $\gamma\gamma\to\pi^+\pi^-$ amplitude. The theorem, however, applies to the amplitude $\gamma^*(q)\gamma^*(-q)\to\pi^+(0)\pi^-(0)$ which is unrelated to $\gamma\gamma\to\pi^+\pi^-$: it involves different chiral coupling constants.

[5] It is likely that the phase-shift determinations in the region $E\gtrsim1.5$ GeV must be updated [64, 65]. This region plays a minor role in our analysis

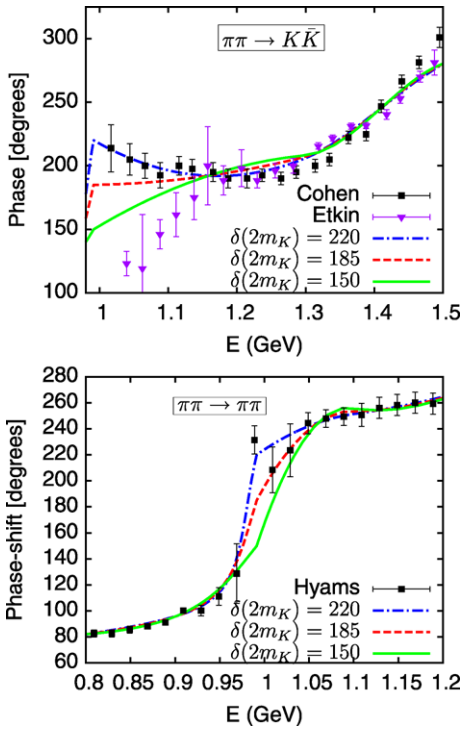

Fig. 4 Fits to the $\pi\pi \to K\bar{K}$ phase (*upper figure*) and the $\pi\pi$ phase-shifts corresponding to different input values of the $K\bar{K}$ threshold phase

simple description of the $\pi\pi$ phase-shift, involving a Breit–Wigner term plus a linear background:

$$\delta_{\pi\pi}(\sqrt{s}) = a + bs + \arctan\frac{m_0\Gamma_0}{m_0^2 - s},$$
$$0.8\ \text{GeV} \le \sqrt{s} \le 2m_K. \tag{81}$$

Assuming given values for the phase-shift at $E = 0.8$ GeV and $E = 2m_K$ fixes the parameters a, b in terms of m_0, Γ_0. These two parameters are then fitted to the experimental data in this region. A few values corresponding to different inputs for the threshold phase $\delta_{\pi\pi}(2m_K)$ are collected in Table 4. The mass and width of the $f_0(980)$ resonance in this simple parametrization are in reasonable agreement with the PDG values. The width is seen to be rather sensitive to the input threshold phase. The corresponding curves are shown on Fig. 4. At energies above $2m_K$, we describe both the $\pi\pi \to \pi\pi$ and $\pi\pi \to K\bar{K}$ phase-shifts by piecewise polynomial functions fitted to experiment.

The modulus of $T_{12}(s)$ it needed in the unitarity equations (17) in the unphysical region $4m_\pi^2 \le s \le 4m_K^2$. Using analyticity and elastic unitarity it can be determined by the MO method. Since the left-hand cut of $T_{12}(s)$ can be expressed in terms of $\pi K \to \pi K$ phase-shifts this MO equation is actually one component of the set of coupled Roy–Steiner equations (see e.g. [71]). We will employ here a simplified but reasonably accurate representation,

Table 4 Mass and width (in GeV) of the $f_0(980)$ resonance arising from fitting the parametrization (81) to the data in the range 0.8 GeV $\le E \le 2m_K$ with different threshold phase inputs

$\delta_{\pi\pi}(2m_K)$	180°	200°	210°	220°
m_0 (GeV)	0.987	0.984	0.983	0.981
Γ_0 (GeV)	0.056	0.039	0.033	0.028

$$T_{12}(s) = \big(A_0 + s\big(A + Bs + Cs^2\big)\big) \times \exp\left[\frac{s}{\pi}\int_{4m_\pi^2}^{\infty} ds'\,\frac{\delta_{12}(s')}{s'(s'-s)}\right] \tag{82}$$

where the two parameters A and A_0 are chosen so as to reproduce the values $T_{12}(0) = 0.097$ and its derivative $\dot{T}_{12}(0) = 1.126\ \text{GeV}^{-1}$ obtained from the full Roy–Steiner equations [71] and the two remaining parameters B and C are fitted to the experimental data in the range [1–1.5] GeV.

The modulus of T_{12} displays a peak associated with the $f_0(980)$ resonance. As one can expect from the formula (82), the size of this peak is strongly correlated with the value of the threshold phase $\delta_{12}(m_K)$. This is illustrated in Fig. 5. The incompatibility between the results of Cohen et al. and of Etkin et al. below $E \simeq 1.2$ GeV is also apparent on this figure. Under the assumption of two-channel unitarity, T_{12} is related to the inelasticity parameter $\eta_{\pi\pi}$ in $\pi\pi$ scattering by

$$T_{12}(s) = \frac{\sqrt{1-\eta^2(s)}}{2\sqrt{\sigma_\pi(s)\sigma_K(s)}} \tag{83}$$

with $\sigma_P(s) = \sqrt{1 - 4m_P^2/s}$. The results of Hyams et al. [41] on the $\pi\pi$ inelasticity which have relatively large error bars are compatible with both Refs. [68, 69]. Once the 2×2 T-matrix is defined, the corresponding 2×2 Omnès matrix can be computed numerically (see [36, 37] for details).

For the D-wave, we have relied on the two-channel K-matrix representation of Hyams et al. [41] for representing the $\pi\pi$ phase-shift, updating the mass and width of the $f_2(1270)$ resonance to the PDG values. In this case the $K\bar{K}$ inelastic channel is not the physically dominant one below 1.3 GeV but is used as an effective description of inelasticity. Furthermore, the inelasticity quoted by the PDG at the energy of the $f_2(1270)$ is significantly smaller than the one obtained by Hyams et al. In practice, we have used a one-channel Omnès representation using the T-matrix phase instead of the S-matrix phase in the inelastic region.

I = 2:

In this case we have ignored inelasticity. For the S-wave, we use the Roy parametrization of Ref. [63] below 0.8 GeV and make a simple fit to the data of Refs. [72, 73] at higher

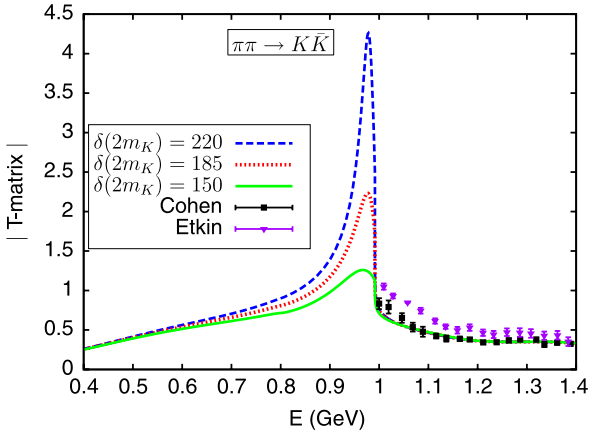

Fig. 5 Modulus of the $\pi\pi \to K\bar{K}$ S-wave T-matrix element using the representation (82) fitted to the data, for several values of the $K\bar{K}$ threshold phase-shift

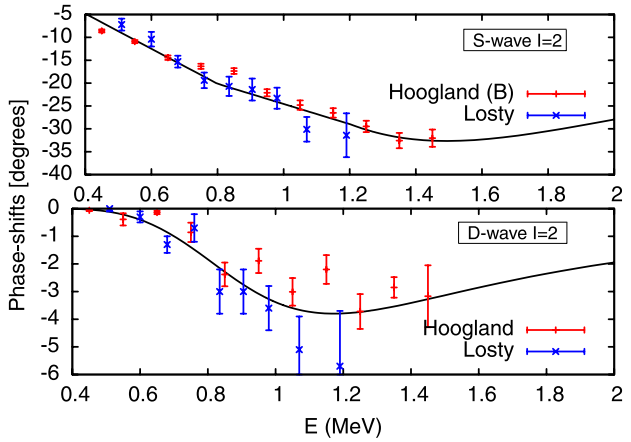

Fig. 6 $\pi\pi \to \pi\pi$ isospin $I = 2$ phase-shifts: S-wave (*upper curve*) and D-wave (*lower curve*)

energy. For the D wave we make a simple fit to the data found in the same references in the whole energy region. These fits are shown in Fig. 6.

6.2 Experimental data

The main body of experimental data which we used are described in the publications [6, 7] (charged pions) and [8, 9] (neutral pions) by the Belle collaboration. They have measured differential cross sections in the range $\cos\theta \leq 0.6$ for $\pi^+\pi^-$ and $\cos\theta \leq 0.8$ for $\pi^0\pi^0$. We have taken into account all their data in the energy range $E \leq 1.28$ GeV i.e. 520 data points for $\pi^0\pi^0$ and 1152 data points for $\pi^+\pi^-$. In addition we have taken into account earlier experimental measurements of cross sections integrated over $\cos\theta$ (in the same ranges as indicated above) from the Crystall Ball collaboration [74] ($\pi^0\pi^0$) as well as MarkII and Cello [75, 76] ($\pi^+\pi^-$). We have assigned equal weights to all the data points. Obviously then, the χ^2 is completely dominated by Belle's results.

6.3 Parameters to be fitted

The dispersive representations for the partial-wave amplitudes as written in Sect. 3 involve 10 subtraction parameters. Not all of them will be determined from the fit.

1. For the $I = 2$ D-waves we have actually assumed an unsubtracted dispersion relation (i.e. the corresponding parameters $c^{(2)}$ and $d^{(2)}$ are determined from sum rules, see (32)).
2. We ave used some chiral constraints. Firstly, we have fixed the parameter $b_K^{(0)}$ to be equal to its ChPT expression at one loop,

$$b_K^{(0)} = -\frac{(L_9^r + L_{10}^r)}{F_\pi^2} + O(p^6). \tag{84}$$

Taking L_9 and L_{10} from Table 2 of Ref. [77] gives

$$b_K^{(0)} \simeq -0.40 \pm 0.30. \tag{85}$$

As a further constraint we use the known value of the $O(p^6)$ coupling c_{34}^r, as discussed in Sect. 5.2. This provides one relation among the seven remaining parameters and leaves six parameters to be fitted. Finally, we perform the fits also imposing that the dipole polarizability difference of the charged pion lies in the range allowed by ChPT [54].

7 Results of the fit

Differential cross sections for $\gamma\gamma \to \pi^0\pi^0$ and $\gamma\gamma \to \pi^+\pi^-$ are evaluated with the $J = 0$ and the $J = 2$ amplitudes computed as explained in Sects. 3, 4, 6. For $\gamma\gamma \to \pi^+\pi^-$ all the $J \geq 4$ amplitudes corresponding to the Born term are also included. The values of the χ^2 results after minimization, corresponding to the various data sets, and adding the statistical and the systematic errors in quadrature, are shown in Table 5. These numbers correspond to a choice of left-cut cutoff $\Lambda_L = -5$ GeV^2 and $K\bar{K}$ threshold phase $\delta(2m_K) = 200°$. The values of the χ^2 for the various data sets are similar (which indicates compatibility) with the exception of the Mark II data [75], which show some deviation. This feature was observed also in some previous analysis [78]. In more detail, the ability of our constrained dispersive representations to reproduce the experimental data is illustrated on Fig. 7 (for $\pi^0\pi^0$) and Fig. 8 (for $\pi^+\pi^-$).

The $\pi^0\pi^0$ amplitude is somewhat simpler than the $\pi^+\pi^-$ one due to the absence of the direct Born contribution in that case. This can be seen from the shapes of the differential cross sections. In the energy region under consideration here

Table 5 χ^2 results from the constrained six parameters fit

	N_{data}	χ^2/N_{data}
$\pi^0\pi^0$ Belle	520	1.26
$\pi^0\pi^0$ Crystal Ball	21	1.13
$\pi^+\pi^-$ Belle	1152	1.39
$\pi^+\pi^-$ Cello	23	1.23
$\pi^+\pi^-$ Mark II	67	2.85

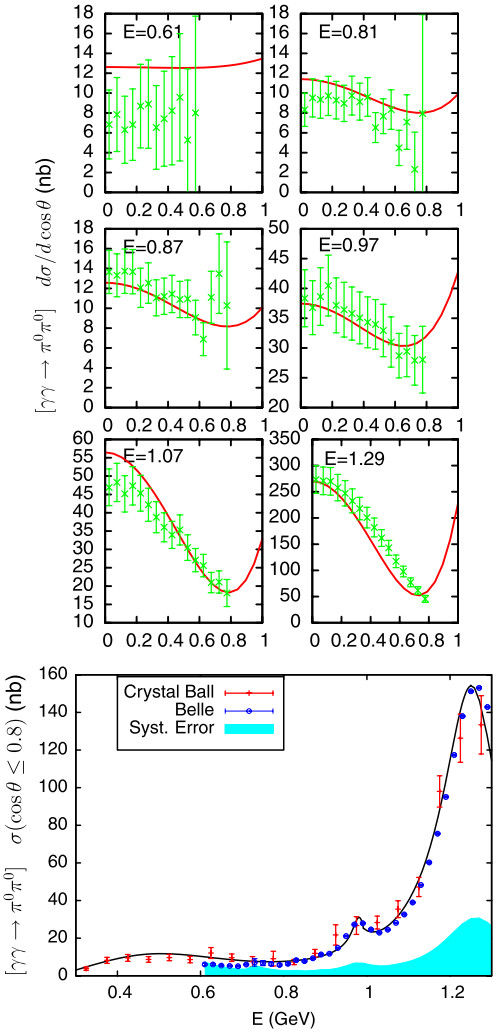

Fig. 7 Differential cross sections (systematic and statistical errors added in quadrature) and integrated cross section (Belle's systematic errors are shown separately) for $\gamma\gamma \to \pi^0\pi^0$. The *solid line* is the result of our constrained fit

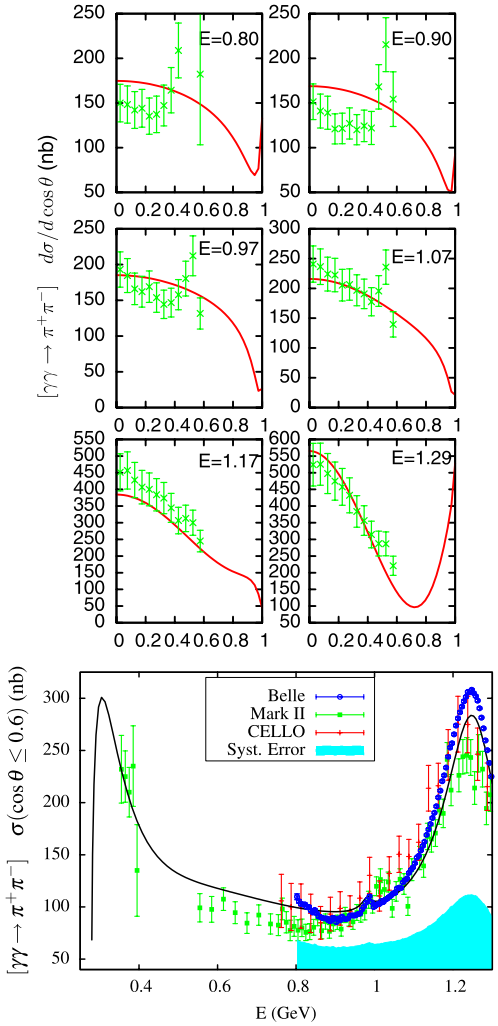

Fig. 8 Same as Fig. 7 for $\gamma\gamma \to \pi^+\pi^-$

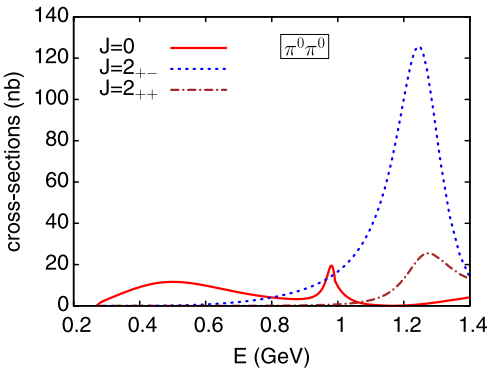

Fig. 9 Contributions from the S and the D partial waves to the $\gamma\gamma \to \pi^0\pi^0$ integrated cross section

only the S-wave and two D-waves effectively contribute to the $\gamma\gamma \to \pi^0\pi^0$ amplitude. In the energy region of the $f_2(1280)$ a significant contribution from the S-wave background is needed for reproducing the experimental cross section. Our S-wave amplitude based on two-channel unitarity cannot be quantitatively trusted in this region. Figure 9 illustrates the role of the various partial waves in the integrated cross section.

The dispersive representations are based on over-subtracted dispersion relations. Assuming reasonable high-

Table 6 Comparison of the subtraction parameters as determined from a fit of the experimental data and as determined from sum rules, as a function of the cutoff Λ_L on the left-cut integration. Units are in appropriate powers of GeV

	$b'^{(0)}$	$b'^{(0)}_K$	$b'^{(2)}$	c^0	d^0
Fit	−7.99	−7.16	3.47	0.22	−0.48
Sum Rule					
$\Lambda_L = -5$	−6.00	−5.61	3.29	0.19	−0.54
$\Lambda_L = -3$	−7.62	−6.84	3.22	0.10	−0.57

energy behavior, five of the subtraction parameters could be written as sum rules (see Sect. 3.1). In practice, the result of such sum rules depend on the cutoff Λ_L that one introduces on the left-hand cut integration (since the precise behavior of the integrand for large negative s is not known). Table 6 shows the numerical (central) values of these parameters, as generated by the fit, and the sum-rule evaluations. The table shows that, for physically reasonable values of the cutoff, $\Lambda_L \simeq -3, -5$ GeV^2, the fitted values are qualitatively in agreement with the sum-rule ones.

• $f_0(980)$ **region:**

Our parametrization of the input $\pi\pi$ phase-shifts allows for some freedom to vary the value of the phase-shift at the $K\bar{K}$ threshold. While the overall χ^2 is hardly sensitive to this small energy region, Belle's data provide a detailed picture of the $f_0(980)$ peak because of the large statistics. A comparison of our results corresponding to different values of the threshold phase-shift $\delta(2m_K)$, with Belle's data, is illustrated on Fig. 10. For clarity of the figure, the systematic errors are not shown, in this region they are of the order of 12 nb for $\pi^+\pi^-$ and 3.5 nb for $\pi^0\pi^0$. In the case of $\pi^0\pi^0$, comparison with the data favors values of the threshold phase $\delta(2m_K) \gtrsim 180°$: for smaller values the peak is too flat and displaced to the right. The value $\delta(2m_K) \simeq 200°$ eventually provides the closest agreement with the experimental peak. The shape of the $f_0(980)$ in $\pi^0\pi^0$ and in $\pi^+\pi^-$ is predicted to differ because of the different sign of the interference between the $I = 0$ resonant amplitude and $I = 2$ amplitude. There is some indication of this feature in the data. Comparing the MO results with the central values of the data for $\pi^+\pi^-$ one must keep in mind that the systematics are larger than for $\pi^0\pi^0$. However, essentially the same value of the threshold phase $\delta(2m_K) \simeq 200°$ also provides the best agreement with the shape of the $f_0(980)$ peak. When $\delta(2m_K)$ gets smaller than $\simeq 170°$ the structure resembles a cusp rather than a peak. Belle's statistics are very high for $\pi^+\pi^-$ and the energy bins $\Delta E = 5$ MeV are smaller than the spacing between the $K^0\bar{K}^0$ and the K^+K^- thresholds ($\simeq$8 MeV, the two thresholds are indicated by arrows in Fig. 10). Belle's data are compatible with a small isospin breaking at the $K\bar{K}$ threshold since agreement with

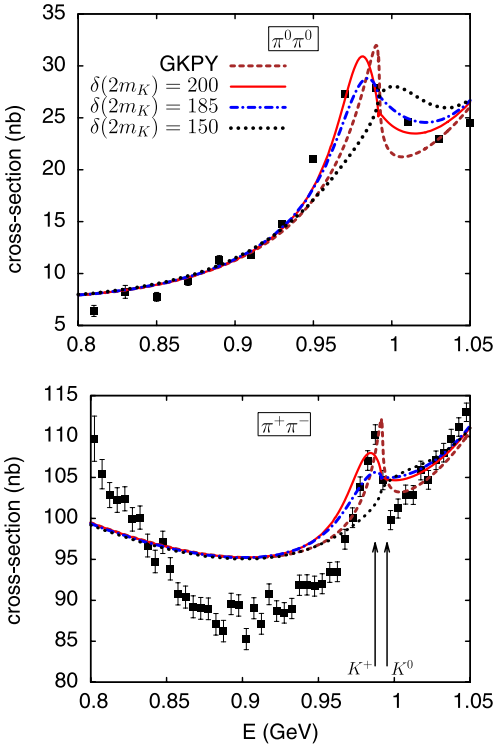

Fig. 10 Integrated cross sections in the region of the $f_0(980)$ peak. The *solid*, *dashed* and *dotted curves* are the result of our MO representation corresponding to three values of the $\pi\pi$ phase-shift at the $K\bar{K}$ threshold. The *long-dashed curves* correspond to using the phase-shifts of Ref. [67]. The experimental results of Belle [6, 8] are shown with their statistical errors only

the MO amplitude (which has no isospin breaking) in this region is not worse than elsewhere. A strong isospin breaking scenario has been proposed by Au et al. [70], according to which the $\pi\pi \to K\bar{K}$ phase drops very sharply in between the two thresholds. Such a scenario is also not ruled out by Belle's data. Isospin breaking near the $K\bar{K}$ threshold involves $a_0(980) - f_0(980)$ mixing. Studies of how this affects the shape of the $a_0(980)$ peak have been performed (e.g. [79, 80]).

• **Low-energy region, pion polarizabilities**

Next, we consider the low-energy region. Figure 11 shows our result for the integrated cross sections in this region and also shows, for comparison, the result from ChPT calculations at NLO and NNLO. As another comparison, we show in Fig. 12 the amplitude $H_{++}(s)/s$ in the subthreshold region normalized as in Fig. 8 of Ref. [51] (above the threshold the modulus is shown). In this region, the dispersive amplitude lies rather close to the chiral amplitudes. In particular, it has an Adler zero close to $s = m_\pi^2$ as has been anticipated in Ref. [22]. The differences between the dispersive results and ChPT are to be attributed to effects of chiral order $O(p^8)$ and also to some differences in $O(p^6)$ coupling constants (see below).

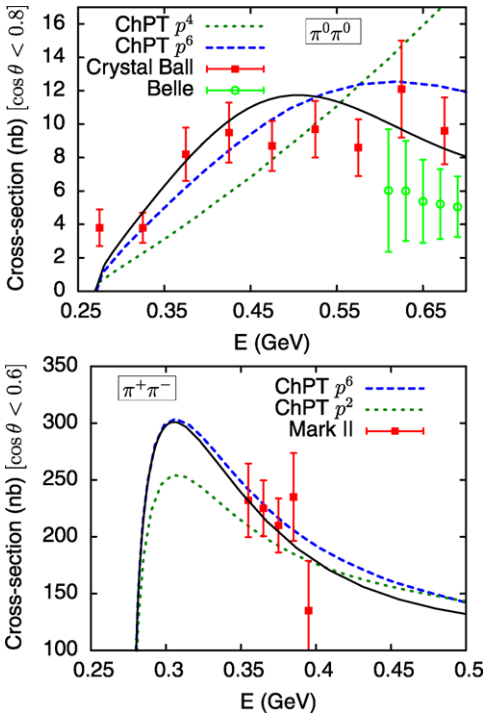

Fig. 11 Integrated $\gamma\gamma$ cross sections at low energy. The experimental results from [74, 75] are shown and also the results from ChPT calculations as given in [53, 54]. The *solid line* is the result from the MO amplitudes

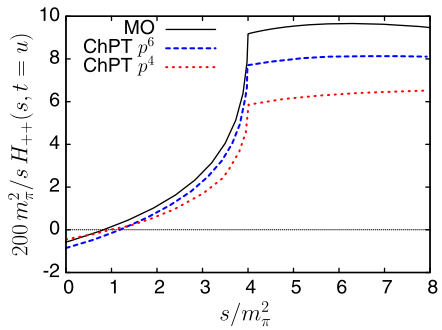

Fig. 12 Amplitude $H_{++}(s, t = u)/s$ in the sub-threshold region and $|H_{++}(s, t = u)|/s$ above the threshold (as in Fig. 8 of Ref. [51]) compared to ChPT results

Expanding the $\gamma\gamma$ amplitudes around $s = 0$ with $t = m_\pi^2$, one accesses pion polarizabilities (see Sect. 5). The results for these quantities deduced from our fitted amplitudes are collected in Table 7 and compared with the results from ChPT at NNLO as given in [53, 54]. Our fit was performed with the constraint that for the charged pion, the polarizability difference $(\alpha_1 - \beta_1)_{\pi^+}$ should lie within the range of the ChPT calculation. The fit prefers the lowest value in the allowed range. This trend differs from the result of Fil'kov and Kashevarov [82] who fitted the charged amplitude only. For the neutral pion, we have imposed a constraint between the dipole and the quadrupole polarizabilities (see (78)). The result for the polarizability difference $(\alpha_1 - \beta_1)_{\pi^0}$ is then in acceptable agreement with the ChPT prediction. Our results for the dipole polarizability sums are in agreement with ChPT. For the quadrupole polarizability differences, our results are slightly smaller than ChPT. This corresponds to somewhat different results for the chiral coupling constant combinations a_1^r, a_2^r and b^r for which simple models have been used in Refs. [53, 54]. Table 8 shows the values of these constants resulting from the fit and compared with those from a resonance model and also from the ENJL model [81]. We note that, in the NJL model, the dipole and quadrupole polarizabilities can be calculated directly, e.g. [83, 84]. Our predictions differ from $O(p^6)$ ChPT for the sums of the quadrupole polarizabilities. The $O(p^6)$ chiral couplings cancel out in the expressions of these observables. As a consequence, they are expected to be sensitive to effects of chiral order p^8 [54]. Let us also mention that our results for $(\alpha_2 - \beta_2)_{\pi^0,\pi^+}$ are somewhat smaller than those obtained in Refs. [82, 85],

$$\begin{aligned}(\alpha_2 - \beta_2)_{\pi^0} &= (39.70 \pm 0.02) \times 10^{-4}\ \text{fm}^5,\\ (\alpha_2 - \beta_2)_{\pi^+} &= \left(25.0^{+0.8}_{-0.3}\right) \times 10^{-4}\ \text{fm}^5\end{aligned} \tag{86}$$

from fitting subtracted dispersive representations (they used a combination of s-fixed and t-fixed dispersion relations) of $\gamma\gamma \to \pi^+\pi^-$ (Ref. [82]), $\gamma\gamma \to \pi^0\pi^0$ (Ref. [85]), amplitudes to experimental data. This difference in the results is to be attributed, we believe, to our combining $\pi^0\pi^0$ and $\pi^+\pi^-$ data in the fits as well as our using a more sophisticated treatment of the final-state interaction in the S-wave, which plays a crucial role for polarizability differences. Our results for the quadrupole polarizability sums $(\alpha_2 + \beta_2)_{\pi^0,\pi^+}$, which

Table 7 Results for dipole and quadrupole polarizabilities (in units of 10^{-4} fm^3 and 10^{-4} fm^5 respectively) of the π^0 and π^+ compared with the values from ChPT at $O(p^6)$ associated with a model for the LEC's (from Ref. [53] for the π^0, and [54] for the π^+. The numbers in brackets correspond to using the ENJL model [81] for the LEC's). The central values shown correspond to a fit with a left integration cutoff $\Lambda_L = -5$ GeV^2. The first error corresponds to the variation of the input parameters and the second error reflects the uncertainties in the experimental $\gamma\gamma$ data

π^0	Fit	ChPT
$(\alpha_1 - \beta_1)_{\pi^0}$	$-1.25 \pm 0.08 \pm 0.15$	-1.9 ± 0.2
$(\alpha_1 + \beta_1)_{\pi^0}$	$1.22 \pm 0.12 \pm 0.03$	1.1 ± 0.3
$(\alpha_2 - \beta_2)_{\pi^0}$	$32.1 \pm 0.9 \pm 1.9$	37.6 ± 3.3
$(\alpha_2 + \beta_2)_{\pi^0}$	$-0.19 \pm 0.02 \pm 0.01$	0.04
π^+		
$(\alpha_1 - \beta_1)_{\pi^+}$	4.7	5.7 ± 1.0
$(\alpha_1 + \beta_1)_{\pi^+}$	$0.19 \pm 0.09 \pm 0.03$	0.16[0.16]
$(\alpha_2 - \beta_2)_{\pi^+}$	$14.7 \pm 1.5 \pm 1.4$	16.2[21.6]
$(\alpha_2 + \beta_2)_{\pi^+}$	$0.11 \pm 0.03 \pm 0.01$	-0.001

Table 8 Values of the three combinations of $O(p^6)$ coupling constants at the scale $\mu = 0.77$ GeV involved in the $\gamma\gamma \to \pi^0\pi^0$ amplitude (second and third row) and in the $\gamma\gamma \to \pi^+\pi^-$ amplitude (fourth and fifth row). The values from a resonance model used in Refs. [53, 54] and from the ENJL model [81] are compared with the values deduced from our fitted dispersive amplitudes. Errors are as in Table 7

π^0	a_1^r	a_2^r	b^r
Fit	$-25.9 \pm 1.6 \pm 3.7$	$8.6 \pm 0.8 \pm 1.8$	$3.4 \pm 0.4 \pm 0.1$
Res. mod. [ENJL]	-39 ± 4 [-23.3]	13 ± 2 [14.9]	3 ± 0.5 [1.7]
π^+	$\tilde{a}_1^r$	$\tilde{a}_2^r$	$\tilde{b}^r$
Fit	-25.0 ± 2.2	$1.4 \pm 1.8 \pm 1.4$	$0.2 \pm 0.3 \pm 0.1$
Res. mod. [ENJL]	-3.2 [-8.7]	0.7 [5.9]	0.4 [0.4]

are controlled by the D-waves, are in rather good agreement with [82, 85].

• Errors

The errors quoted in Tables 7, 8 have been estimated as follows. The uncertainties associated with the description of the left-hand cut has been evaluated by varying all the input coupling constants as well as the integration cutoff Λ which was varied between -3 and -10 GeV^2. Concerning the final-state interaction, we have varied the $\pi\pi$ scattering lengths ($a_0^0 = 0.220 \pm 0.005$, $a_0^2 = -0.0444 \pm 0.0010$) and used, below $E = 1$ GeV two different representations for the $I = 0$ S-wave $\pi\pi$ phase-shift [63, 67]. We have also varied the resonance parameters in the D-wave. Concerning the errors in the fitted parameters, the usual criterion based on increasing the χ^2 by one unit is based on the assumption that the experimental errors are statistical and that the correlation matrix is known. These assumptions are not valid in the present case. We have therefore adopted a more phenomenological criterion, considering the χ^2 per point instead of the total one and allowing it to increase by 0.5. The errors associated with the fitted parameters and those associated with the input data are quoted separately in Tables 7, 8. The π^+ polarizability difference $(\alpha_1 - \beta_1)_{\pi^+}$ is not completely determined by the fit as it lies at the boundary of the allowed value. No error can be quoted in this case. Correspondingly, we quote a single error for the LEC combination $\tilde{a}_1^r$ in Table 8.

8 Conclusions

We have reconsidered the MO dispersive representations of photon–photon scattering amplitudes and applied them to the recent results of the Belle collaboration [6–9]. This method is general and follows from the non-perturbative features of QCD. Its range of applicability can be extended up to slightly above 1 GeV by taking into account the main source of inelasticity in $\pi\pi$ scattering. Our description of the left-hand cut includes the contributions of the vector, axial-vector as well as tensor resonances i.e. all relevant resonances with masses up to 1.3 GeV. We found that the tensor resonances play a significant role in the left-hand cut. We employ MO representations somewhat different from previous works, keeping the left-cut parts in the form of spectral integrals. In this manner, one avoids polynomial ambiguities associated with propagators of particles with non-zero spin. Furthermore, the spectral function displays in a clear way how a regularization occurs in exchanges of resonances of different types.

We have also argued that chiral constraints can be imposed on the subtraction constants using model independent information on p^6 chiral couplings. We have shown that a sum rule on a single p^6 parameter for $\pi^0\pi^0$ provides a non trivial constraint. Making use of all these theoretical constraints, one obtains an amplitude containing only six parameters. We introduce a cutoff on the left-cut spectral integration, accounting for a Regge-type regularization, but no other cutoff. In contrast to e.g. Refs. [28, 32], the QED Born term is used unmodified by form-factors.

We have fitted the subtraction parameters to a data set containing 541 points on $\gamma\gamma \to \pi^0\pi^0$ and 1242 points on $\gamma\gamma \to \pi^+\pi^-$. This set is largely dominated by Belle's results. We find good compatibility between Belle data on $\pi^0\pi^0$ and the lower energy data from the Crystal Ball collaboration. In the case of $\pi^+\pi^-$ we find compatibility between the data from Belle and the data from Cello as well as the data from MarkII below 0.4 GeV. The compatibility with the MarkII data in the range 0.4–1.0 GeV is more marginal.

In the region of the $K\bar{K}$ threshold and the $f_0(980)$ peak, we find reasonable agreement between Belle's data and our parametrization which assumes a smooth isospin limit. The charged channel, however, does not rule out the possibility of some isospin violating effects in the shape of the peak. The cross sections around the peak in both the neutral and charged channels are best reproduced for values of the threshold phase $\delta(2m_K) \simeq 200^\circ \pm 20^\circ$. From our calculation we also obtain the amplitude $\gamma\gamma \to K\bar{K}$ for $I = J = 0$. It is unfortunately difficult to probe this part against the exper-

imental data on $\gamma\gamma \to K^+\bar{K}^-, K^0\bar{K}^0$ since the experimental amplitudes contain admixtures from isospin $I = 1$.

We have shown that Belle's data are compatible with the pion polarizabilities predicted in ChPT. In the case of the π^0 we have derived a refined value. We have also derived results for the quadrupole polarizabilities of both the charged and neutral pion. Our results for the differences $\alpha_2 - \beta_2$ are somewhat smaller than those derived in Refs. [82, 85]. We believe this to be due to our using more precise $\pi\pi$ phase-shifts at low energies for the S-waves. It is clear, however, that experimental data on photon–photon scattering at low energies (i.e. below 0.5 GeV) are most efficient for determining pion polarizabilities with precision. It is hoped that such experiments will be performed at facilities like KLOE2 or BESIII.

Acknowledgements The authors would like to thank the Belle collaboration and especially prof. S. Uehara for sending us their experimental results and for correspondence. We also thank prof. B. Ananthanarayan for carefully reading the manuscript and for comments. This work is supported in part by the EU Contract No. MRTN-CT-2006-035482 FLAVIAnet and by the EU project HadronPhysics2.

References

1. J. Bijnens, G. Colangelo, G. Ecker, Ann. Phys. **280**, 100 (2000). arXiv:hep-ph/9907333
2. J. Bijnens, G. Colangelo, G. Ecker, J. High Energy Phys. **9902**, 020 (1999). arXiv:hep-ph/9902437
3. G. Colangelo, Nucl. Phys. A **827**, 228C (2009)
4. J. Ahrens et al., Eur. Phys. J. A **23**, 113 (2005). arXiv:nucl-ex/0407011
5. A. Guskov (COMPASS Collaboration), Fizika B **17**, 313 (2008)
6. T. Mori et al. (Belle Collaboration), J. Phys. Soc. Jpn. **76**, 074102 (2007). arXiv:0704.3538 [hep-ex]
7. T. Mori et al. (Belle Collaboration), Phys. Rev. D **75**, 051101 (2007). arXiv:hep-ex/0610038
8. S. Uehara et al. (Belle Collaboration), Phys. Rev. D **78**, 052004 (2008). arXiv:0805.3387 [hep-ex]
9. S. Uehara et al. (BELLE Collaboration), Phys. Rev. D **79**, 052009 (2009). arXiv:0903.3697 [hep-ex]
10. J.R. Batley et al. (NA48/2 Collaboration), Eur. Phys. J. C **54**, 411 (2008)
11. J.R. Batley et al. (NA48/2 Collaboration), Phys. Lett. B **633**, 173 (2006). arXiv:hep-ex/0511056
12. J.R. Batley et al. Eur. Phys. J. C **64**, 589 (2009)
13. B. Adeva et al. (DIRAC Collaboration), Phys. Lett. B **619**, 50 (2005). arXiv:hep-ex/0504044
14. S. Pislak et al. (BNL-E865 Collaboration), Phys. Rev. Lett. **87**, 221801 (2001). arXiv:hep-ex/0106071
15. R. Oehme, Int. J. Mod. Phys. A **10**, 1995 (1995). arXiv:hep-th/9412040
16. R. Omnès, Nuovo Cimento **8**, 316 (1958)
17. N.I. Muskhelishvili, *Singular Integral Equations* (Noordhof, Groningen, 1953)
18. M. Gourdin, A. Martin, Nuovo Cimento **17**, 224 (1960)
19. R.L. Goble, J.L. Rosner, Phys. Rev. D **5**, 2345 (1972)
20. R.L. Goble, R. Rosenfeld, J.L. Rosner, Phys. Rev. D **39**, 3264 (1989)
21. D. Morgan, M.R. Pennington, Phys. Lett. B **192**, 207 (1987)
22. D. Morgan, M.R. Pennington, Phys. Lett. B **272**, 134 (1991)
23. J.F. Donoghue, B.R. Holstein, Phys. Rev. D **48**, 137 (1993). arXiv:hep-ph/9302203
24. J.F. Donoghue, B.R. Holstein, Y.C. Lin, Phys. Rev. D **37**, 2423 (1988)
25. J. Bijnens, F. Cornet, Nucl. Phys. B **296**, 557 (1988)
26. K. Sundermeyer, A coupled channel analysis of the reactions gamma + Gamma → Pi + Pi And Gamma + Gamma → K + Anti-K. Preprint DESY 74/17
27. O. Babelon, J.L. Basdevant, D. Caillerie, M. Gourdin, G. Mennessier, Nucl. Phys. B **114**, 252 (1976)
28. Y. Mao, X.G. Wang, O. Zhang, H.Q. Zheng, Z.Y. Zhou, Phys. Rev. D **79**, 116008 (2009). arXiv:0904.1445 [hep-ph]
29. G. Mennessier, Z. Phys. C **16**, 241 (1983)
30. M. Boglione, M.R. Pennington, Eur. Phys. J. C **9**, 11 (1999). arXiv:hep-ph/9812258
31. J.A. Oller, L. Roca, C. Schat, Phys. Lett. B **659**, 201 (2008). arXiv:0708.1659 [hep-ph]
32. N.N. Achasov, G.N. Shestakov, Phys. Rev. D **77**, 074020 (2008). arXiv:0712.0885 [hep-ph]
33. G. Mennessier, S. Narison, W. Ochs, Phys. Lett. B **665**, 205 (2008). arXiv:0804.4452 [hep-ph]
34. A.R. Edmonds, *Angular Momentum in Quantum Mechanics* (Princeton University Press, Princeton, 1960)
35. M. Jacob, G.C. Wick, Ann. Phys. **7**, 404 (1959) [Ann. Phys. **281**, 774 (2000)]
36. J.F. Donoghue, J. Gasser, H. Leutwyler, Nucl. Phys. B **343**, 341 (1990)
37. B. Moussallam, Eur. Phys. J. C **14**, 111 (2000). arXiv:hep-ph/9909292
38. F.E. Low, Phys. Rev. **96**, 1428 (1954)
39. M. Gell-Mann, M.L. Goldberger, Phys. Rev. **96**, 1433 (1954)
40. H.D.I. Abarbanel, M.L. Goldberger, Phys. Rev. **165**, 1594 (1968)
41. B. Hyams et al., Nucl. Phys. B **64**, 134 (1973). AIP Conf. Proc. **13**, 206 (1973)
42. C. Amsler et al. (Particle Data Group), Phys. Lett. B **667**, 1 (2008)
43. P. Ko, Phys. Rev. D **41**, 1531 (1990)
44. G. Ecker, J. Gasser, A. Pich, E. de Rafael, Nucl. Phys. B **321**, 311 (1989)
45. S. Godfrey, N. Isgur, Phys. Rev. D **32**, 189 (1985)
46. B. Collick et al., Phys. Rev. Lett. **53**, 2374 (1984)
47. M. Zielinski et al., Phys. Rev. D **30**, 1855 (1984)
48. G.T. Condo, T. Handler, W.M. Bugg, G.R. Blackett, M. Pisharody, K.A. Danyo, Phys. Rev. D **48**, 3045 (1993)
49. M. Nozar et al. (CLAS Collaboration), Phys. Rev. Lett. **102**, 102002 (2009). arXiv:0805.4438 [hep-ex]
50. H.J. Lipkin, Phys. Lett. B **72**, 249 (1977)
51. S. Bellucci, J. Gasser, M.E. Sainio, Nucl. Phys. B **423**, 80 (1994) [Erratum: Nucl. Phys. B **431**, 413 (1994)]. arXiv:hep-ph/9401206
52. U. Bürgi, Nucl. Phys. B **479**, 392 (1996). arXiv:hep-ph/9602429
53. J. Gasser, M.A. Ivanov, M.E. Sainio, Nucl. Phys. B **728**, 31 (2005). arXiv:hep-ph/0506265
54. J. Gasser, M.A. Ivanov, M.E. Sainio, Nucl. Phys. B **745**, 84 (2006). arXiv:hep-ph/0602234
55. K. Maltman, C.E. Wolfe, Phys. Rev. D **59**, 096003 (1999). arXiv:hep-ph/9810441
56. S. Dürr, J. Kambor, Phys. Rev. D **61**, 114025 (2000). arXiv:hep-ph/9907539
57. M. Knecht, B. Moussallam, J. Stern, Nucl. Phys. B **429**, 125 (1994). arXiv:hep-ph/9402318
58. J. Gasser, C. Haefeli, M.A. Ivanov, M. Schmid, Phys. Lett. B **675**, 49 (2009). arXiv:0903.0801 [hep-ph]
59. G. Amorós, J. Bijnens, P. Talavera, Nucl. Phys. B **568**, 319 (2000). arXiv:hep-ph/9907264
60. H. Terazawa, Phys. Rev. Lett. **26**, 1207 (1971)
61. B.R. Martin, D. Morgan, G. Shaw, *Pion–Pion Interactions in Particle Physics* (Academic Press, London, 1976)

62. S.M. Roy, Phys. Lett. B **36**, 353 (1971)
63. B. Ananthanarayan, G. Colangelo, J. Gasser, H. Leutwyler, Phys. Rep. **353**, 207 (2001). arXiv:hep-ph/0005297
64. D.V. Bugg, B.S. Zou, A.V. Sarantsev, Nucl. Phys. B **471**, 59 (1996)
65. R. Kamiński, L. Leśniak, K. Rybicki, Z. Phys. C **74**, 79 (1997). arXiv:hep-ph/9606362
66. R. Kamiński, J.R. Peláez, F.J. Ynduráin, Phys. Rev. D **77**, 054015 (2008). arXiv:0710.1150 [hep-ph]
67. R. García-Martín, R. Kamiński, J.R. Peláez, F.J. Ynduráin, arXiv:0906.5467 [hep-ph]
68. D.H. Cohen, D.S. Ayres, R. Diebold, S.L. Kramer, A.J. Pawlicki, A.B. Wicklund, Phys. Rev. D **22**, 2595 (1980)
69. A. Etkin et al., Phys. Rev. D **25**, 1786 (1982)
70. K.L. Au, D. Morgan, M.R. Pennington, Phys. Rev. D **35**, 1633 (1987)
71. P. Büttiker, S. Descotes-Genon, B. Moussallam, Eur. Phys. J. C **33**, 409 (2004). arXiv:hep-ph/0310283
72. M.J. Losty et al., Nucl. Phys. B **69**, 185 (1974)
73. W. Hoogland et al., Nucl. Phys. B **126**, 109 (1977)
74. H. Marsiske et al. (Crystal Ball Collaboration), Phys. Rev. D **41**, 3324 (1990)
75. J. Boyer et al., Phys. Rev. D **42**, 1350 (1990)
76. H.J. Behrend et al. (CELLO Collaboration), Z. Phys. C **56**, 381 (1992)
77. G. Ecker, Acta Phys. Pol. B **38**, 2753 (2007). arXiv:hep-ph/0702263
78. M.R. Pennington, T. Mori, S. Uehara, Y. Watanabe, Eur. Phys. J. C **56**, 1 (2008). arXiv:0803.3389 [hep-ph]
79. N.N. Achasov, G.N. Shestakov, Phys. Rev. D **70**, 074015 (2004). arXiv:hep-ph/0405129
80. C. Hanhart, B. Kubis, J.R. Peláez, Phys. Rev. D **76**, 074028 (2007). arXiv:0707.0262 [hep-ph]
81. J. Bijnens, J. Prades, Nucl. Phys. B **490**, 239 (1997). arXiv:hep-ph/9610360
82. L.V. Fil'kov, V.L. Kashevarov, Phys. Rev. C **73**, 035210 (2006). arXiv:nucl-th/0512047
83. V. Bernard, D. Vautherin, Phys. Rev. D **40**, 1615 (1989)
84. B. Hiller, W. Broniowski, A.A. Osipov, A.H. Blin, Phys. Lett. B **681**, 147 (2009). arXiv:0908.0159 [hep-ph]
85. L.V. Fil'kov, V.L. Kashevarov, Phys. Rev. C **72**, 035211 (2005). arXiv:nucl-th/0505058